IMMUNOLOGY

Self-assembling peptide nanofiber HIV vaccine elicits robust vaccine-induced antibody functions and modulates Fc glycosylation

Jui-Lin Chen[1,2]†, Chelsea N. Fries[3]‡, Stella J. Berendam[1], Nicole S. Rodgers[4], Emily F. Roe[3], Yaoying Wu[3], Shuk Hang Li[5], Rishabh Jain[3], Brian Watts[1], Joshua Eudailey[6], Richard Barfield[7,8], Cliburn Chan[7,8], M. Anthony Moody[1,9], Kevin O. Saunders[1,4], Justin Pollara[1,4], Sallie R. Permar[6], Joel H. Collier[3]*, Genevieve G. Fouda[1,9]*

To develop vaccines for certain key global pathogens such as HIV, it is crucial to elicit both neutralizing and non-neutralizing Fc-mediated effector antibody functions. Clinical evidence indicates that non-neutralizing antibody functions including antibody-dependent cellular cytotoxicity (ADCC) and antibody-dependent cellular phagocytosis (ADCP) contribute to protection against several pathogens. In this study, we demonstrated that conjugation of HIV Envelope (Env) antigen gp120 to a self-assembling nanofiber material named Q11 induced antibodies with higher breadth and functionality when compared to soluble gp120. Immunization with Q11-conjugated gp120 vaccine (gp120-Q11) demonstrated higher tier 1 neutralization, ADCP, and ADCC as compared to soluble gp120. Moreover, Q11 conjugation altered the Fc N-glycosylation profile of antigen-specific antibodies, leading to a phenotype associated with increased ADCC in animals immunized with gp120-Q11. Thus, this nanomaterial vaccine strategy can enhance non-neutralizing antibody functions possibly through modulation of immunoglobulin G Fc N-glycosylation.

INTRODUCTION

Accumulating evidence suggests that key global pathogens, such as HIV, for which vaccine development has been challenging, may require vaccine strategies that can induce both neutralizing and non-neutralizing antibody functions (*1*–*6*). Since the discovery of antibodies with extensive neutralization breadth [known as broadly neutralizing antibodies (bnAbs)] against HIV strains elicited by natural infection, the induction of this type of antibodies has been the ultimate goal of HIV vaccinologists (*7*). However, efforts to develop bnAb-inducing vaccines against HIV have been unfruitful thus far. Notably, the RV144 vaccine trial achieved a moderate 31.2% efficacy, without elicitation of neutralizing responses against circulating strains. This observation suggests that the moderate protection achieved by the RV144 vaccine was mediated by non-neutralizing antibody responses (*8*, *9*). A number of studies have shown that non-neutralizing antibody functions such as antibody-dependent cellular phagocytosis (ADCP) and antibody-dependent cellular cytotoxicity (ADCC) are crucial for controlling HIV (*1*), influenza (*2*), herpes simplex virus (*3*), Ebola virus (*4*), and cytomegalovirus (CMV) (*5*, *6*). A follow-up study to the RV144 trial (HVTN 702) using a similar vaccine strategy in Africa was recently discontinued because of lack of efficacy (*10*), and although more investigation is needed to understand the differences between HVTN 702 and RV144, the discrepancy is suggestive that an optimal HIV vaccine may require elicitation of both neutralizing and non-neutralizing antibody responses.

Although non-neutralizing antibody functions are regulated by multiple factors, posttranslational glycosylation of Asn^{297} (N-glycosylation) in the antibody heavy chain constant domain 2 (CH2) domain is a crucial modulator of Fc-mediated effector functions (*11*, *12*). N-glycosylation can be diversified by fucosylation, single or double galactosylation, addition of bisecting *N*-acetylglucosamine, or sialylation of galactose via two different linkages (fig. S1) (*13*, *14*). This structural heterogeneity of N-glycosylation results in the selective engagement of different classes of Fc receptors associated with Fc-mediated functions (*13*, *15*). While it has been reported recently that certain types of adjuvants can influence antibody sialylation (*16*), current strategies for modulating antibody glycosylation through vaccination are still limited.

Nanomaterials represent a novel class of vaccine platforms that present potential advantages for HIV vaccine design (*17*). Notably, nanomaterials such as liposomes, virus-like particles, and ferritin nanoparticles, among others, have shown the ability to increase the neutralization potency of HIV vaccine–elicited antibodies in animal models (*18*–*20*). Although, to date, nanomaterial-based HIV vaccines have not successfully induced bnAbs, it appears that nanomaterials can improve the quality of antibody responses (*17*). In previous work, we have demonstrated that nanofibers formed from the β sheet self-assembling peptide Q11 are a useful vaccine platform for tailoring adaptive immune responses (*21*–*25*). Q11 nanofibers have self-adjuvanting properties (*26*, *27*) and also allow for controlled

[1]Duke Human Vaccine Institute, Duke University School of Medicine, Durham, NC 27710, USA. [2]Department of Molecular Genetics and Microbiology, Duke University School of Medicine, Durham, NC 27710, USA. [3]Department of Biomedical Engineering, Duke University, Durham, NC 27708, USA. [4]Department of Surgery, Duke University School of Medicine, Durham, NC 27710, USA. [5]The Cell and Molecular Biology Graduate Group, University of Pennsylvania, Philadelphia, PA 19104, USA. [6]Department of Pediatrics, Weill Cornell Medicine, New York, NY 10065, USA. [7]Department of Biostatistics and Bioinformatics, Duke University School of Medicine, Durham NC 27710, USA. [8]Center for Human Systems Immunology, Duke University School of Medicine, Durham, NC 27707, USA. [9]Department of Pediatrics, Duke University School of Medicine, Durham, NC 27710, USA.
*Corresponding author. Email: joel.collier@duke.edu (J.H.C.); genevieve.fouda@duke.edu (G.G.F.)
†Present address: Department of Pediatrics at Weill Cornell Medicine, 525 E 68th St., New York, NY 10065, USA.
‡Present address: University of Washington, 3946 W Stevens Way NE, Seattle, WA 98195, USA.

valency of conjugated peptides or proteins over several orders of magnitude (*24*, *28*, *29*). Antigen valency has been shown to influence trafficking of immunogens to B cell follicles in vivo and for activating rare, low-affinity B cell lineages (*17*, *30*–*32*), so an ability to control valency in supramolecular peptide nanofibers is advantageous within HIV vaccine design.

In a recent study, we demonstrated that conjugating the HIV gp120 antigen to Q11 nanofibers induced antibody responses with stronger binding to heterologous HIV Envelope (Env) antigens than soluble gp120 in immunized mice and that enhancement of the antibody response was driven by the multivalent presentation of gp120 (*33*). Here, we immunized rabbits with Q11-conjugated gp120 (gp120-Q11) to evaluate the functional profile of vaccine-elicited antibodies. Rabbits were chosen as the primary animal model in this study because rabbits are phylogenetically closer to humans as compared to mice (*34*). In addition, higher volumes of blood can be collected, allowing assessment of antibody functions. Moreover, rabbit antibodies can bind human Fc receptors, which allows measurement of Fc-dependent functions such as ADCC and ADCP with human effector cells (*34*). We demonstrated that conjugation of gp120 to Q11 increased neutralization to autologous tier 1 virus and ADCP and ADCC responses. Moreover, we found a correlation between enhanced ADCC responses and the Fc glycosylation profiles induced by gp120-Q11 vaccine, which suggests that supramolecular nanofiber presentation of antigens can modulate the phenotype of vaccine-elicited antibody responses via modification of the Fc glycosylation profile.

RESULTS

Sortase-driven Q11 conjugation preserved bnAb epitopes

We previously demonstrated that a peptide termed β tail can slowly transition from an α helix to a β sheet conformation and coassemble with Q11 nanofibers even when conjugated to a folded protein (*28*, *35*). With such property, β tail serves as a versatile tool for incorporating folded protein antigens in nanofibers formed by self-assembling β sheet peptides. In this study, we adapted this conjugation system for displaying gp120 from a subtype C strain CH505 on Q11 nanofibers. Briefly, gp120 was first ligated to a poly-glycine–β tail peptide (G_{15}–β tail) via a sortase-mediated reaction (*36*), followed by coassembly with Q11 peptides to form gp120-Q11 nanofibers (Fig. 1A). The morphology of the resultant gp120-Q11 vaccine was examined with transmission electron microscopy (TEM) (Fig. 1B), and the gp120 content in gp120-Q11 was quantified by SDS–polyacrylamide gel electrophoresis (fig. S2, A and B). Both circular dichroism (fig. S3A) and thioflavin T fluorescence assay (fig. S3B) confirmed the

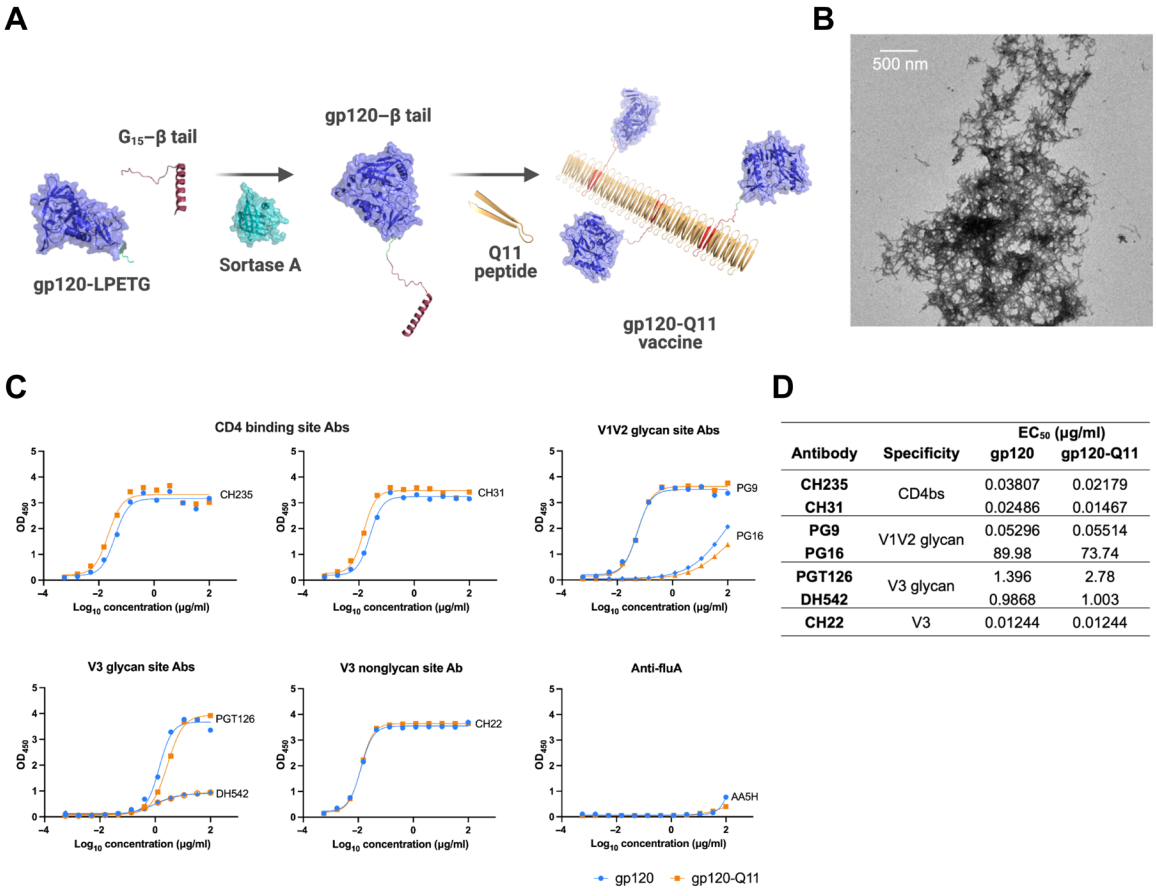

Antibody	Specificity	EC50 (μg/ml) gp120	EC50 (μg/ml) gp120-Q11
CH235	CD4bs	0.03807	0.02179
CH31		0.02486	0.01467
PG9	V1V2 glycan	0.05296	0.05514
PG16		89.98	73.74
PGT126	V3 glycan	1.396	2.78
DH542		0.9868	1.003
CH22	V3	0.01244	0.01244

Fig. 1. Sortase-mediated conjugation of gp120 to Q11 nanofibers preserved bnAb epitopes. Nanofiber vaccines were constructed using sortase A–mediated conjugation. (**A**) Schematic of gp120-Q11 conjugation (created with PyMOL and Biorender.com). (**B**) On TEM grids, gp120-Q11 nanofibers stained with uranyl acetate formed laterally aggregated assemblies of nanofibers. (**C** and **D**) Comparable binding of gp120 and gp120-Q11 to bnAbs targeting distinct bnAbs epitopes. (C) Binding curves. (D) Table of EC_{50} values using sigmoidal curve fitting. OD_{450}, optical density at 450 nm.

presence of β sheet secondary structures in the gp120-Q11 vaccine after mixing with STR8S-C adjuvant. Combined with TEM imaging, this result indicates that the structure of Q11 nanofiber was not compromised by the process of protein conjugation or by STR8S-C. To assess the antigenicity of gp120 after conjugation to Q11 nanofibers, we used enzyme-linked immunosorbent assay (ELISA) to test its binding to several different HIV bnAbs. We observed that gp120-Q11 bound multiple different bnAbs with similar 50% effective concentration (EC_{50}) values as compared to unconjugated gp120 (Fig. 1C). Notably, the binding curves of V2 glycan–dependent (PG9 and PG16) and V3 glycan–dependent (PGT126 and DH542) bnAbs to gp120-Q11 and unmodified gp120 were nearly superimposable (Fig. 1, C and D), indicating that the conformational protein and glycan structures were preserved using the sortase-mediated conjugation chemistry. Overall, these results indicate that sortase-mediated conjugation of gp120 to Q11 nanofibers preserves binding to relevant Env bnAb epitopes.

gp120-Q11 vaccine induced robust antibody binding to heterologous Env antigens and to HIV-infected cells

The magnitude and breadth of HIV Env–specific binding antibodies were assessed in rabbits immunized either with gp120-Q11 or with gp120 (Fig. 2A). Because of their ability to induce robust antibody responses, Toll-like receptor (TLR) agonist adjuvants are now commonly used in HIV vaccine research (*37*, *38*). We therefore adjuvanted both gp120 and gp120-Q11 vaccine groups with STR8S-C, a squalene-based emulsion adjuvant containing the TLR agonists R848 and CpG (CpG oligodeoxynucleotide) (*39*). We previously reported that STR8S-C can induce strong antibody binding and ADCC responses

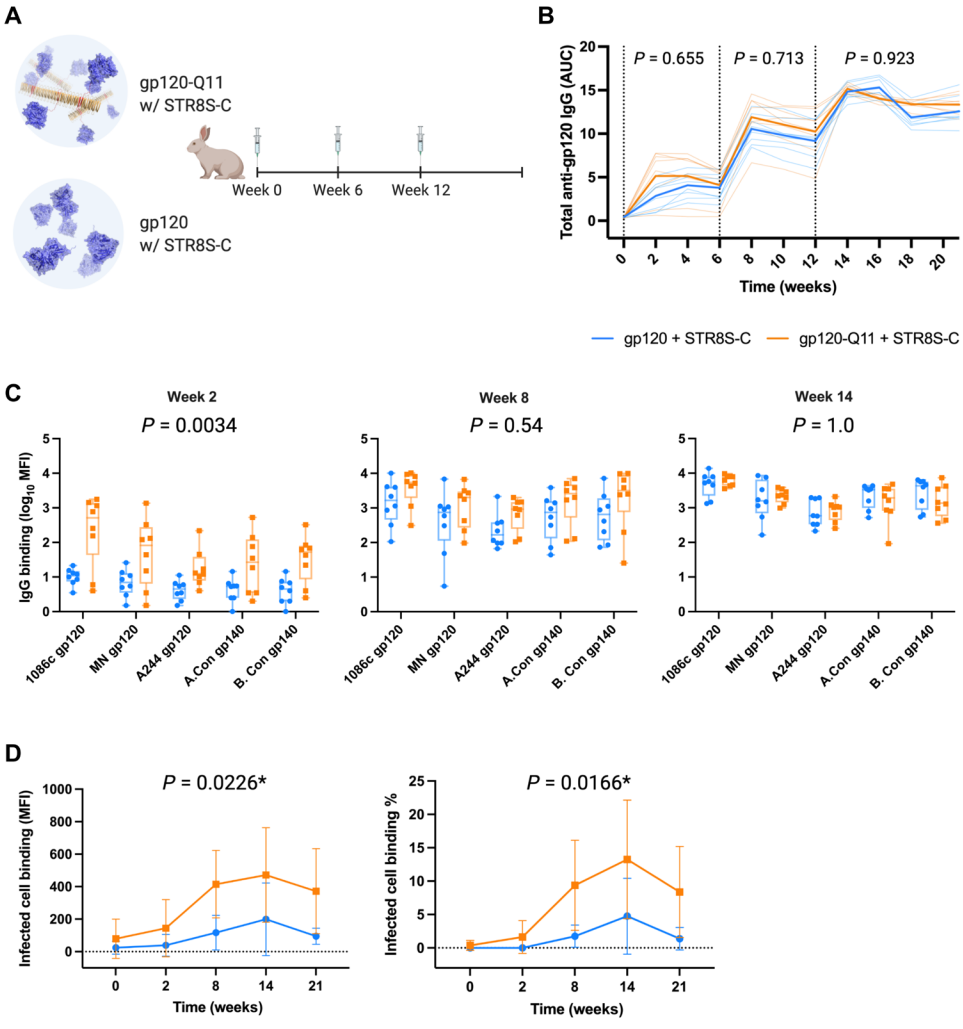

Fig. 2. Nanofiber-conjugated gp120 elicited the early development of antibodies capable of binding to cross-clade heterologous HIV antigens and to virus-infected cells. (**A**) Vaccination schedule: Rabbits were immunized subcutaneously with three doses of vaccine consisting of 15 μg of either gp120 ($n = 8$) or gp120-Q11 ($n = 8$). Both groups were adjuvanted with STR8S-C (image created with Biorender.com). (**B**) Magnitude of binding antibody responses to the vaccine antigen (CH505 Con gp120) was similar between gp120-Q11 and gp120 vaccine groups. Antibody response is presented as area under the curve (AUC) with the immunization time points indicated as vertical dotted lines. Group means are indicated by bold lines, and individual animals are represented as thin lines. *P* values were computed using a linear mixed effect model with week 0 excluded in the analysis. (**C**) Binding to heterologous HIV Envs at weeks 2, 8, and 14 was measured by binding antibody multiplexed assay (BAMA). *P* values were computed using generalized estimating equations (GEE). MFI, median fluorescence intensity. (**D**) Serum antibody binding to CEM.NKR_{CCR5} cells infected with the CH505T/F infectious molecular clone virus is presented as MFI (left) and the percentage of cells bound by antibodies (right). The mean ± SD is presented. *P* values were computed using a nonparametric repeated measures test [week 0 was excluded in the test, *FDR (false discovery rate) $P < 0.1$].

in nonhuman primates (*39*). Rabbits immunized with gp120 and gp120-Q11 developed similar magnitudes of binding antibodies against the autologous Env, CH505 Con gp120, following each immunization (Fig. 2B). In rabbits immunized with gp120-Q11, the antibody response to Q11 scaffold was also measured. After three doses of gp120-Q11, the level of immunoglobulin G (IgG) against Q11 was elevated slightly compared to before vaccination ($P = 0.016$; fig. S4). However, the IgG level against gp120 at the same time point was 29-fold higher than anti-Q11 IgG ($P = 0.0078$). This result is consistent with our previous observations in mice immunized with Q11-conjugated gp120 (*33*) and ovalbumin peptide (*27*), suggesting that Q11 is minimally immunogenic in both species.

Although antibody magnitude to gp120 was similar between the two groups, gp120-Q11 broadened the ability of the vaccine-induced antibodies to bind to heterologous Envs early in the immunization regimen compared to soluble gp120. After a single dose of gp120-Q11, a robust binding response to heterologous HIV Envs was observed, whereas a comparable response was only detected in the gp120 group after two vaccine doses (Fig. 2C). This result suggests that the nanofiber vaccine may have activated a broader set of naïve B cells than soluble gp120. To further probe the vaccine-induced antibody binding response, we measured the antibody binding to cells infected with HIV CH505 transmitted/founder (T/F) infectious molecular clone virus, an in vitro model that resembles natural infection. Higher levels of binding were observed in the gp120-Q11 vaccine group throughout the immunization regimen (Fig. 2D and fig. S5). This observation suggests an enhanced binding capacity induced by gp120-Q11 vaccination as compared to soluble gp120. Consistent with previous findings in mice (*33*), these results reinforce the importance of valency in enhancing antibody binding responses to HIV glycoprotein antigens.

Nanofiber conjugation enhanced antibody functions, including ADCC and ADCP

To explore the functional profile of vaccine-elicited antibodies, we measured neutralization, ADCP, and ADCC. After three doses of gp120 vaccines, animals immunized with gp120 and gp120-Q11 developed low levels of neutralization against the autologous tier 1 virus CH505 w4.3 (*40*), and these levels were slightly higher in the gp120-Q11 group (Fig. 3A). Neutralization was completely abrogated after IgG depletion (Fig. 3A), suggesting that the low levels of neutralization were mediated by IgG.

Studies have shown that Fc-mediated functions (e.g., ADCP and ADCC) contribute to postinfection control of HIV and other viruses (*1*–*4*), so we assessed the ability of the vaccines to induce ADCP and ADCC. To measure ADCP, we used human monocyte-origin cell line THP-1 as the effector cells and fluorescent microspheres coupled either to the autologous CH505T/F gp120 or to heterologous 1086.C gp120 as targets (*41*, *42*). The level of ADCP against the autologous gp120 was comparable between the two vaccine groups, whereas a higher level of ADCP activity against 1086.C gp120 was observed in the gp120-Q11 group following immunization (Fig. 3B). This result is consistent with the increased binding breath observed in the gp120-Q11 group (Fig. 2C). ADCC was measured against CEM.NKR_{CCR5} cells infected with HIV CH505T/F and against cells coated with CH505T/F gp120 (*43*). Notably, gp120-Q11 elicited higher antibody titers and higher magnitude of ADCC (Fig. 3C), suggesting that the quantity and quality of ADCC-inducing antibodies were promoted by gp120-Q11 immunization. Improved responses were not limited to gp120-coated cells but were also observed against HIV-infected cells (Fig. 3C). As both ADCP and ADCC functions depend on Fc-FcR interactions, the observation of stronger ADCP and ADCC responses following gp120-Q11 vaccination suggests that there may be differences in the Fc characteristics of antibodies induced by gp120-Q11 and soluble gp120.

gp120-Q11 vaccine induced a distinct humoral response profile as compared to soluble gp120

To compare different immunological features across the vaccine groups, we normalized data to *z* scores and visualized them with a heatmap. We unbiasedly analyzed the data of autologous and heterologous Env binding, infected-cell binding, and all the different functions formerly presented here to comprehensively profile the magnitude, breadth, and the functionality of antibodies induced by gp120 and gp120-Q11. The heatmap reiterates the observation of enhanced vaccine-elicited antibody binding response and effector functions in the animals immunized with gp120-Q11 vaccine (Fig. 3D). In addition, we applied principal component analysis (PCA) to analyze the dataset presented in Fig. 3D, as PCA is an unbiased tool to identify the similarity (clustering) within the data, and it can also point out the factors that differentiate clusters (*44*). gp120-immunized animals form a single cluster and differentiate from most of the animals in the gp120-Q11 group on Dim 1 (Fig. 3E). ADCP and heterologous Env binding were the two major contributors to Dim 1, followed by ADCC to gp120-coated cells and infected-cell binding (fig. S6). Rabbits 9 and 10 locate on the opposite ends of both Dim 1 and 2 away from other gp120-Q11 rabbits, suggesting that these two rabbits demonstrated the opposite trend of humoral response. By analyzing the top contributors to Dim 1 and Dim 2 (fig. S6) and complementing the PCA plot with the heatmap (Fig. 3D), we found that rabbits 9 and 10 showed stronger binding and ADCC responses to infected cells and neutralization yet weaker binding to heterologous Envs. In contrast, animal 11 demonstrated a stand-alone case where gp120-Q11 induced robust heterologous Env binding, Fc functions, and neutralization. This suggests that it is possible to improve both neutralizing and Fc-mediated antibody functions by scaffolding gp120 on Q11 nanofibers.

Q11 vaccine induced higher levels of fucosylated and monogalactosylated IgG in rabbits and mice

Because glycosylation on residue N279 regulates Fc-mediated antibody functions, including ADCC and ADCP (*13*), we investigated the impact of Q11 conjugation on the Fc glycosylation profile of gp120-specific IgG and total serum IgG using capillary electrophoresis (fig. S7) (*45*). Rabbits represent an ideal animal model for assessing the impact of Fc N-glycosylation because they have only one IgG subclass, which eliminates the confounding factor of different IgG subclasses in analyzing antibody functionality (*46*). After three doses (week 14) of vaccines, different glycosylation profiles of gp120-specific IgG induced by gp120-Q11 and gp120 can be observed on the heatmap (Fig. 4A) and along clustering in the PCA plot (Fig. 4B). In the gp120-specific analysis at week 14, gp120 and gp120-Q11 groups show higher degree of separation along Dim 1, where glycoforms G1FB[6]/G1F[3], A1F(2,6), G1FS1(2,6), G1[6], G2F, A1FB (2,6), G1[3], and G1F[6] were the top contributors (fig. S8A). A lesser degree of clustering can be observed in total IgG at week 14 with similar groups of contributor to Dim 1 and Dim 2 as compared to gp120-specific IgG (fig. S8B). This result suggests that

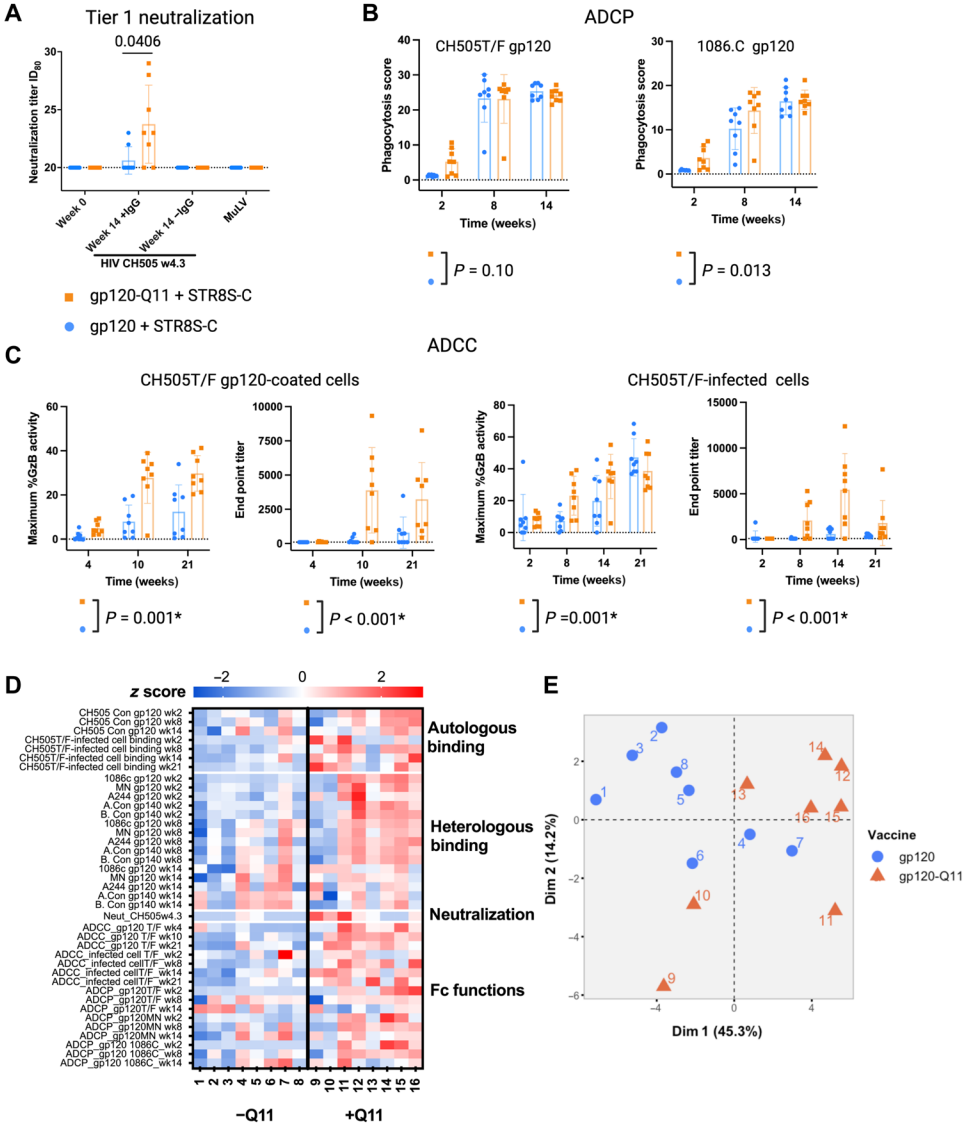

Fig. 3. Nanofiber-conjugated gp120 induced a distinct functional profile, featuring higher tier 1 neutralizing antibody responses and ADCC. (**A**) Neutralization of the tier 1 CH505 w4.3 pseudotyped virus measured by TZM-bl cell neutralization assay. IgG-depleted serum (−IgG) was used as control to confirm that neutralization was mediated by IgG. Neutralization against the control murine leukemia virus (MuLV) was also assessed. Bars indicate the group mean with error bars presenting the SD (Wilcoxon test). ID_{80}, 80% inhibitory dose. (**B**) ADCP against the autologous Env and the heterologous clade C 1086.C gp120. GEE was applied to compare vaccine groups across all time points. (**C**) gp120-Q11 vaccine induced a stronger ADCC response against gp120-coated cells (left) and CH505T/F-infected cells (right). *P* values were computed using a nonparametric repeated measures test. Permutation approach was applied because of singular covariance matrix (*FDR $P < 0.1$). GzB, granzyme B. (**D**) *z* score was used for comparison between different immunological variables in animals immunized with gp120-Q11 (+Q11) and gp120 (−Q11). (**E**) PCA revealed that animals 9, 10, and 11 in the gp120-Q11 vaccine group demonstrated distinct functional profile from the other animals within the same vaccine group, whereas gp120 vaccine induced a more homogeneous functional profile.

the clustering in vaccine groups observed in total serum IgG glycosylation might result from the gp120-specific IgG, as it was not depleted in total IgG in glycosylation analysis.

To dissect the features of glycosylation induced by gp120 and gp120-Q11, we analyzed the levels of fucosylation, sialylation, bisection, and galactosylation of the IgG in both vaccine groups. gp120-Q11 induced higher levels of fucosylation, bisection, and monogalactosylation (Fig. 4C). In contrast, the glycosylation profiles of total IgG at weeks 0 and 14 were comparable between the two vaccine groups (fig. S9).

To assess whether the ability of Q11 to modulate IgG glycosylation was specific to rabbits or whether it extended to other mammalian species, we analyzed samples from our previous study in which wild-type mice were immunized with three doses of 1086.C gp120-Q11 or 1086.C gp120. Both groups were also adjuvanted with STR8S-C (Fig. 5A) (*33*). Similar to rabbits, gp120-specific IgG antibodies from mice immunized with gp120-Q11 showed an antibody glycosylation profile that differed from the gp120 vaccine (Fig. 5, B and C). Mice immunized with gp120-Q11 or gp120 demonstrate more separation on Dim 1 (Fig. 5C) with a group of top glycoform contributors

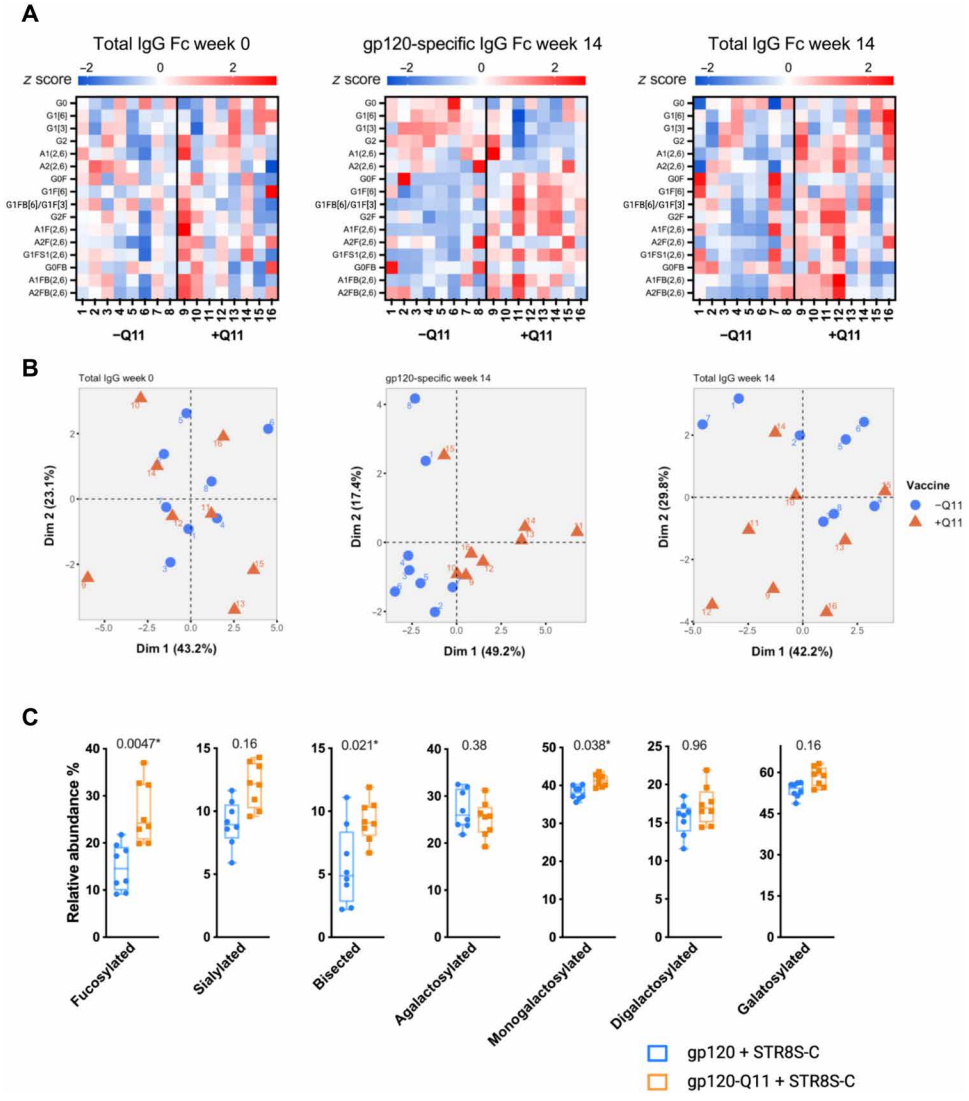

Fig. 4. Nanofiber conjugation modulated gp120-specific IgG Fc glycosylation profile in rabbits. (**A**) gp120-Q11 vaccine induced a distinct glycosylation profile in gp120-specific IgG illustrated as *z* scores on heatmaps showing the glycosylation of week 0 total IgG (left), week 14 gp120-specific IgG (middle), and week 14 total IgG (right; nomenclature of glycan structures can be found in fig. S1). Glycoform G1FB[6] cannot be differentiated from G1F[3] in the assays, so it is presented as G1FB[6]/G1F[3]. (**B**) PCA was applied to complement heatmap visualization. No distinct clustering was observed in total IgG (left) at week 0, whereas a clear separation between gp120-Q11– and gp120-vaccinated rabbits was observed in week 14 gp120-specific IgG (middle) and, to a lesser degree, in week 14 total IgG (right). (**C**) Higher levels of fucosylation, bisection, and monogalactosylation of gp120-specific IgG were induced by gp120-Q11 (Wilcoxon test, normalized with week 0, *FDR $P < 0.1$).

similar to that observed in rabbit gp120-specific IgG with a few exceptions (fig. S10). In mice, glycoforms A2(2,6), A1(2,6), A2F(2,6)/A2FB(2,6), G2, and G0FB are among the top contributors to the Dim 1 in PCA of mouse gp120-specific IgG glycosylation but not in rabbits (fig. S8). Notably, similar to rabbits, higher levels of fucosylation and monogalactosylation of gp120-specific IgG antibodies were observed in mice immunized with gp120-Q11 (Fig. 5D). Although there was no significant difference in overall galactose level between the two groups, gp120-Q11 induced higher levels of agalactosylated and monogalactosylated IgG but lower levels of digalactosylated IgG (Fig. 5D). Similar to rabbit total serum IgG, a comparable total serum IgG Fc glycosylation profile was observed in gp120- and gp120-Q11–immunized mice (fig. S11).

To assess the impact of Q11 nanofiber on antibody glycosylation in the absence of an external adjuvant, we analyzed the IgG glycosylation in mice immunized with unadjuvanted 1086.C gp120 ($n = 5$) or gp120-Q11 ($n = 4$) from our previous study (*33*). Vaccines were given at weeks 0, 2, 5, and 11. Serum from weeks 12 and 14 was pooled together to have enough volume for glycan analysis. Although the difference between gp120 and gp120-Q11 vaccine groups was not statistically significant because of small group sizes, the IgG glycosylation profile induced by gp120-Q11 in the absence of an adjuvant shared a similar trend with gp120-Q11 administrated with STR8S-C (fig. S12A). Higher levels of fucosylation, agalactosylation, and monogalatosylation yet lower level of digalatosylation were induced by gp120-Q11. The lack of statistical significance was likely

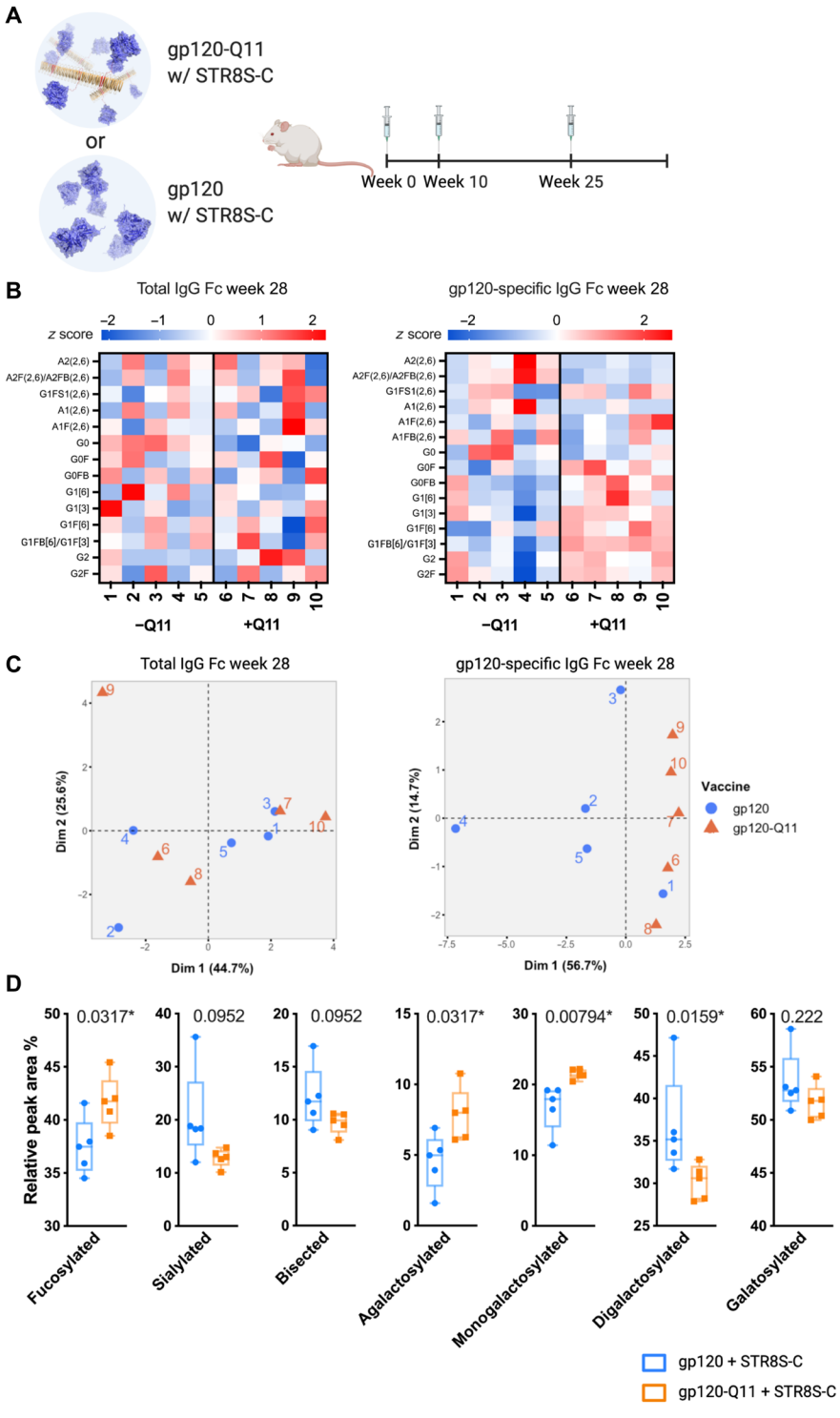

Fig. 5. Q11 nanofiber conjugation also modulated gp120-specific IgG Fc glycosylation in mice following gp120-Q11 vaccination. (**A**) Mice were immunized with three doses of 15 μg of gp120 or gp120-Q11 in the presence of STR8S-C adjuvant (image created with Biorender.com). (**B**) As shown with *z* score on heatmaps, a similar glycosylation profile of total IgG was observed between vaccine groups (left) after three immunizations. In contrast, the glycosylation profile of gp120-specific IgG is distinct in mice immunized with gp120-Q11 IgG (right) as compared to gp120. (**C**) In the PCA of glycan profile, clustering of gp120-Q11 and gp120 vaccine groups can be observed in the gp120-specific IgG but not in the total IgG. (**D**) Higher levels of fucosylation, agalactosylation, and monogalactosylation yet lower levels of digalactosylation of gp120-specific IgG were induced by gp120-Q11 as compared to gp120 (Wilcoxon test, *FDR $P < 0.1$).

at least partly due to the low S/N (signal-to-noise) ratio observed in one animal in each vaccine group, which increased the variation of the data. Therefore, we reanalyzed the same dataset excluding these two animals. After removing these two data points, the trend in each glycan feature became clearer yet still followed the same direction, and notably, all three animals in the gp120-Q11 group showed higher levels of fucosylation than animals in the gp120 group (fig. S12, B and C). The similarity of glycosylation patterns elicited by Q11 vaccines with and without STR8S-C adjuvant suggests that Q11 itself has a substantial impact on antibody fucosylation and galactosylation. In the presence of STR8S-C, gp120-Q11 appeared to induce lower levels of sialylated IgG and bisected IgG (Fig. 5D) despite lack of statistical significance, whereas such pattern was not observed without STR8S-C (fig. S12, A and B). As the levels of sialylation and bisection were higher when STR8S-C was present (Fig. 5D) as compared to unadjuvanted conditions (fig. S12, A and B), it is possible that STR8S-C increased the levels of these two glycan features and Q11 counteracted its effect.

The increase of fucosylated IgG induced by gp120-Q11 was initially unexpected, as it has been previously reported that fucosylation reduces ADCC by impeding Fc binding with Fcγ receptor IIIa (FcγRIIIa) in humans (*47*–*49*). Therefore, to assess the impact of fucosylation on antibody's ability to engage the human FcγRIIIa, we measured the binding of gp120-specific serum antibody to FcγRIIIa and to the inhibitory Fc receptor FcγRIIb in rabbits immunized with gp120-Q11 or gp120. Fucosylation of certain glycan was negatively correlated with antibody binding to FcγRIIIa (fig. S13A). However, no reduced overall antibody binding to FcγRIIIa or increased binding to FcγRIIb was observed in gp120-Q11–immunized rabbits (fig. S13B). To examine the possibility that different levels of downstream cellular signaling were activated despite comparable FcγR binding, we used a FcR signaling assay based on BW5147 cell lines that stably express different FcγRs fused to CD3 intracellular domain (CD3ζ) as previously described (*50*). Consistent with our results of FcR binding, no statistically significant differences was observed between gp120-Q11 and gp120 vaccine groups in activation of FcγRIIIA or FcγRIIb (fig. S13C). Overall, our data suggest that fucosylation of gp120-specific IgG induced by gp120-Q11 immunization may not affect the antibody's interaction with FcγRIIIA or FcγRIIb.

Fucosylation and monogalactosylation of gp120-specific IgG were correlated with ADCC

The influence of Fc glycosylation on effector functions has been extensively studied using monoclonal antibodies. However, little is known about how these functions are regulated by the glycan repertoire of polyclonal antibodies in response to vaccination. Therefore, we analyzed the correlation between Fc-mediated functions and Fc glycosylation in the immunized rabbits. Glycan profile of gp120-specific IgG at week 14 demonstrated strong correlation with ADCC against CH505T/F gp120–coated cells at week 21, while much weaker correlations with ADCC were observed in total IgG glycan at weeks 0 and 14 (Fig. 6A). Notably, monogalactosylation [Spearman ρ, 0.747; 95% confidence interval (CI), 0.366 to 0.904] and fucosylation (0.571; 0.115 to 0.902) showed strong to moderate positive correlation with ADCC (Fig. 6A).

Individual glycoforms G1FS1 (2,6) (0.726; 0.371 to 0.891), A1F (2,6) (0.656; 0.256 to 0.901), A1FB (2,6) (0.668; 0.265 to 0.849), and G1FB[6]/G1F[3] (0.8; 0.521 to 0.954) at week 14 were positively correlated with ADCC, whereas G1[3] (−0.571; −0.91 to −0.021) and G2 (−0.55; −0.865 to −0.0328) were negatively correlated with ADCC (nomenclature of glycan structures can be found in fig. S1; Fig. 6A). In contrast, ADCP activity poorly correlated with glycosylation (fig. S14). Among the 16 individual glycoforms shown in Fig. 6A, ADCC-activating glycans G1FS1 (2,6), A1F (2,6), A1FB (2,6), G0F, and G1FB[6]/G1F[3] were up-regulated in animals immunized with the gp120-Q11 vaccine, while ADCC-inhibiting glycans G1[3] and G2 were down-regulated (Fig. 6B and fig. S15). Comparable avidity to gp120 and epitope specificity were observed between gp120 and gp120-Q11 vaccine groups (fig. S16, A and B); therefore, the increased ADCC observed in the gp120-Q11 group was likely driven by the glycans on Fc region, not by Fab-related factors of the vaccine-induced antibodies. Here, we identified certain individual Fc glycoforms that were correlated with enhanced ADCC. Except for fucosylation, these glycoforms all have different features including bisection, sialylation, and galactosylation that are positively correlated with ADCC. This result suggests that other sugars, not just fucose, on Fc glycan may also be involved in modulating Fc effector functions in the context of polyclonal antibodies.

DISCUSSION

We previously demonstrated that self-assembling nanofiber Q11 vaccines can be used to enhance antibody binding responses to HIV glycoprotein gp120 in mice (*33*). By displaying Env antigens on Q11 nanofibers, antibody responses against homologous and heterologous HIV Env antigens were enhanced. In the present study, we used a similar gp120-Q11 vaccine formulation to explore the landscape of antibody functionality in rabbits, a preclinical animal model that is well suited to assess antibody functions. Similar to our results in mice, we found that the breadth of antibody binding to heterologous HIV Env antigens was higher in gp120-Q11–immunized rabbits after the first dose. These results suggest that Q11 nanofiber conjugation enhances humoral response against gp120 across different mammalian species.

Although comparable binding breadth to heterologous Env antigens was observed between gp120 and gp120-Q11 after two doses of the vaccine, antibodies induced by gp120-Q11 were more capable of engaging the Env antigen expressed on the HIV-infected cells throughout the vaccination regimen. This finding suggest that Q11 modulated the breadth of vaccine-elicited antibodies. This modulation likely occurred through a mechanism that depends on Q11's ability to present multiple copies of gp120, as antigen valency has been reported to play a critical role in diversifying the repertoire of vaccine-elicited antibodies (*17*, *32*, *51*–*53*).

Many studies have demonstrated that passive immunization with bnAbs provides protection against mucosal HIV challenge in nonhuman primates (*54*–*58*), and recent vaccine trials have shown that passive immunization with bnAb VRC01 can provide protection against HIV strains sensitive to this bnAb (*59*). Hence, the induction of bnAbs has been the ultimate goal of modern HIV vaccine designs. In this study, only low levels of neutralizing activity against autologous tier 1 virus were induced by the gp120-Q11 vaccine (Fig. 3A). This result was not unexpected because other gp120-based vaccines such as the bivalent gp120 vaccine (AIDSVAX B/E) used in the RV144 and Vax003 trials also did not induce any tier 2 neutralization (*60*). Nevertheless, it is worth noting that although the levels were low, gp120-Q11 induced higher tier 1 neutralization

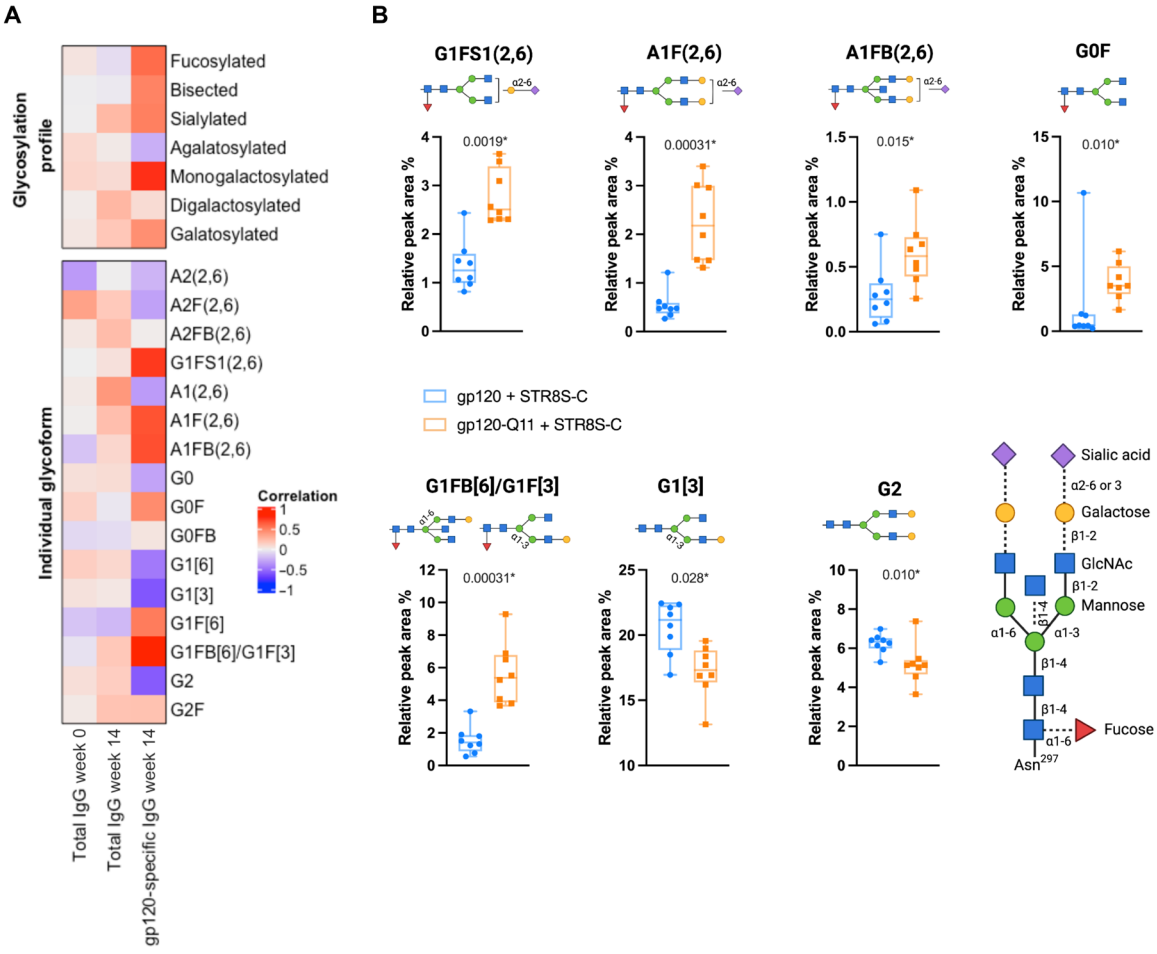

Fig. 6. ADCC-activating glycoforms were up-regulated upon gp120-Q11 immunization in rabbits. (**A**) A higher degree of correlation between ADCC and glycosylation was observed in gp120-specific IgG than in total IgG at weeks 0 and 14. Compared to glycans sharing a common feature (top), the relative abundance of individual glycoforms (bottom) demonstrated stronger correlation with ADCC in general. (**B**) Individual glycoforms that showed medium to strong correlation (positive or negative) with ADCC are graphed to compare the relative abundance of each glycoform in gp120-Q11 and gp120 vaccine groups (Wilcoxon test, *FDR $P < 0.1$). Structure of each glycoform is presented using glycan standard symbols nomenclature (www.ncbi.nlm.nih.gov/glycans/snfg.html): red triangle for fucose, yellow circle for galactose, blue square for *N*-acetylglucosamine, green circle for mannose, and purple diamond for *N*-glycolylneuraminic acid (image created with Biorender.com).

relative to that of soluble gp120. As it is generally believed that the induction of tier 2 neutralization will require immunogens to present epitopes that resembles the native conformation shown on an HIV virion, future work should investigate whether using nanofiber to display native-like trimeric antigens such as SOSIP could enhance the ability of these immunogens to induce heterologous tier 2 neutralization.

Bartsch *et al.* (*16*) demonstrated that TLR agonists such as lipopolysaccharide, MPLA (monophosphoryl-lipid A), R848, and poly(I:C) (polyinosinic-polycytidylic acid) can increase the levels of IgG sialylation and galactosylation. We also observed a similar effect with STR8S-C, a TLR agonist, on mouse IgG glycosylation (Fig. 5C and fig. S12). In addition to increased levels of sialylation and galactosylation, the level of bisection seemed to be up-regulated by STR8S-C and fucosylation seemed to be down-regulated. Therefore, TLR agonists may have a wide effect on antibody glycosylation, yet it is not excluded that the glycosylation pattern that we observed in this study was a result of the combined effect of Q11 nanofiber and STR8S-C adjuvant. Notably, Q11 seems able to induce higher levels of fucosylation and monogalactosylation in different contexts. Besides adjuvantation, we also noted that the antibody glycosylation pattern varied in different species. We found that changes in sialylation, bisection, agalactosylation, and digalactosylation induced by gp120-Q11 in rabbits (Fig. 4C) were opposite to the trends observed in mice (Fig. 5D). Although the mechanism of such difference is still unclear, this result suggests that species respond differently to Q11 nanofiber and/or STR8S-C. Nevertheless, fucosylation and monogalactosylation seem to be consistent at least between rabbits and mice. As very few studies have compared the antibody glycosylation across species, this paper might be the first one to report the similarities and contrasts of antibody glycosylation in different species responding to a multivalent vaccine.

One of the main findings in this study was the enhancement of Fc-mediated antibody functions including ADCP and ADCC after immunization with gp120-Q11 (Fig. 3, B and C). Because non-neutralizing antibody functions reduced the risk of HIV acquisition

in the RV144 trial (*1*), enhancement of ADCC function through Q11 conjugation to HIV Env antigens could be clinically important. The increase in ADCC potency in the gp120-Q11 group was correlated with elevated levels of several fucosylated IgG glycoforms (Fig. 6, A and B). Such a finding seems contradictory to most studies where ADCC function of monoclonal antibodies was associated with lower levels of fucosylation (*47*, *49*, *61*). To validate these findings, we examined the correlation between FcγR binding and different IgG glycoforms. Similar to studies by Li *et al.* (*61*) where monoclonal antibodies were glycoengineered to assess the impact of fucosylation on ADCC and FcγRIIIa binding, we observed that fucosylation of G0, G1, G2, and A1 was negatively correlated with the binding to FcγRIIIa (fig. S13A). However, the higher levels of fucosylation did not affect the overall FcγRIIIa binding or the downstream signaling (fig. S13, B and C). This is probably because other sugars in N-glycan may also influence the interaction with FcγRIIIa, which offsets the impact of fucosylation. Our results suggest possible differences in the mechanisms through which Fc glycosylation regulates ADCC of vaccine-elicited polyclonal antibodies compared to glycoengineered monoclonal antibodies. In general, ADCC was more strongly correlated with the relative abundance of individual glycoforms than with that of glycans sharing common features (e.g., fucosylation; Fig. 6A). Therefore, unlike the conventional fucosylation/defucosylation model, ADCC is more likely to be controlled by the levels of each individual glycoform in in vivo settings. These findings may enable more specific examination of IgG glycoform's impacts on Fc-mediated functions in future vaccine design and evaluation.

The ability to modulate Fc glycosylation through vaccination could present important advantages in tailoring immune responses against target pathogens. Fc fucosylation and sialylation are the key elements in suppressing antibody-induced inflammation (*15*). Despite the success of using afucosylated IgG in enhancing ADCC against cancer (*49*, *62*), natural infections of severe acute respiratory syndrome coronavirus 2 (SARS-CoV-2) and dengue virus have shown that afucosylated IgG can be detrimental in some disease contexts. Elevated levels of afucosylated IgG along with inflammatory markers interleukin-6 (IL-6) and C-reactive protein were found in patients with COVID-19 (coronavirus disease 2019) who developed severe symptoms, whereas these factors were not elevated in asymptomatic or mild self-limiting infections (*63*–*65*). In dengue infection, higher levels of afucosylated IgG1 were found to be associated with the development of dengue hemorrhagic fever (*66*, *67*). Removal of fucose can enhance ADCC response by increasing antibody's affinity to FcγRIIIa (*61*), yet as demonstrated by SARS-CoV-2 and dengue infection, dysregulated FcγRIIIa response can lead to pathogenic, sometimes lethal, inflammatory responses in the context of viral infections. However, our study demonstrates that Q11 as a vaccine carrier can enhance ADCC without increasing the levels of afucosylated IgG (Figs. 3C and 4C).

In summary, we report that a self-assembling nanofiber-based HIV vaccine is able to enhance the breadth of binding antibody response and the functional profile of the vaccine-elicited antibodies. Conjugation of gp120 to Q11 nanofibers also induced changes of N-glycosylation in the vaccine-specific antibodies, and such change was associated with elevated levels of ADCC. To our knowledge, this study described the first evidence of a nanomaterial vaccine modulating antibody glycosylation. Thus, Q11 is a promising vaccine platform for further development in the context of HIV and other challenging pathogen immunogen designs.

MATERIALS AND METHODS

Vaccine synthesis and antigenicity measurement

Subtype C, CH505 strain consensus HIV Env gp120 antigen (CH505 Con gp120) was expressed with sortase enzyme recognition sequence (LPETG) on the C terminus (*43*). To conjugate CH505 gp120 to G_{15}–β tail peptide (G_{15}-MALKVELEKLKSELVVLHSELHKLKSEL), 10.9 μM CH505 gp120 was coincubated with 25 μM sortase A and 60 μM G_{15}–β tail overnight at 4°C (*36*). As sortase A was expressed with poly-histidine tag, we removed it from the mixture after conjugation reaction by using a His SpinTrap column (Cytiva Life Sciences, #28401353). The resultant CH505 gp120–β tail conjugate was mixed with 10 mM Q11 peptide (QQKFQFQFEQQ) aqueous solution in 4:1 ratio (v/v), yielding a final concentration of 2 mM Q11. Overnight incubation allowed coassembly of gp120–β tail and Q11 peptides into nanofibers (*28*). Nanofibers bearing conjugated gp120 were pelleted at 9000*g* to separate assemblies from unassembled proteins in solution, followed by gentle washing with phosphate-buffered saline (PBS) to remove nonspecifically bound protein.

Animal immunization and blood collection

Thirteen-week-old female New Zealand White rabbits (Envigo Global Services Inc.) were subcutaneously immunized either with 15 μg of CH505 Con gp120 with STR8S-C adjuvant (15%, v/v) (*39*) or with 15 μg of CH505 Con gp120-Q11 with STR8S-C. Booster immunizations were administered 6 and 12 weeks after the first immunization. Blood was collected biweekly from the ear central artery, while the animals were sedated with acepromazine (1 mg/kg). Ten female C57BL/6 mice were purchased at 8 weeks of age from the Jackson Laboratory. After 1 week of acclimation, mice were immunized with 15 μg of 1086.C gp120 with STR8S-C (10%, v/v) or 15 μg of 1086.C gp120-Q11 and STR8S-C, as described in the previous study (*33*). Plasma was separated from whole blood by centrifugation at 900*g* for 15 min and stored at −80°C before analysis. All animal handling procedures were conducted following a protocol approved by the Duke University Institutional Animal Care and Use Committee under number A199-21-09.

Antigenicity assessment by ELISA

The ability of a panel of HIV Env monoclonal antibodies (mAbs) to bind to gp120-Q11 was compared to the binding to soluble gp120 as previously described (*33*). Briefly, 384-well polystyrene high-binding ELISA plates (Corning Life Sciences, #3700) were coated with gp120 or gp120-Q11 at a concentration equivalent to 5 μg/ml of gp120 and incubated overnight at 4°C. The next day, the plates were blocked with superblock solution (4% whey, 15% goat serum, and 0.5% Tween 20 in 1× PBS) for 1 hour; then, serial dilutions of the mAbs were added (12 threefold dilutions starting at 100 μg/ml). The panel of mAbs tested included CD4 binding site mAbs CH235 and VRC-CH31, V1V2 glycan mAbs PG9 and PG16, V3 glycan mAbs PGT126 and DH542, V3 mAb CH22, and anti-flu mAb AA5H (Abcam, #ab20343). After an hour of incubation and four washes, horseradish peroxidase (HRP)–conjugated goat anti-human antibody (1:4000; Promega, #W4031) was added. Binding was visualized using the SureBlue TMB Microwell Peroxidase Substrate followed by the TMB stop solution. The plates were then read with a SpectraMax Plus 384 plate reader (Molecular Devices LLC) at a wavelength of 450 nm.

Measurement of vaccine-elicited Env-specific antibodies

Env-specific antibodies were measured by ELISA as aforementioned with the following modifications: 384-well polystyrene high-binding

ELISA plates were coated with CH505 Con gp120 at 5 μg/ml and incubated with rabbit plasma diluted in 1:10 to $1:10^6$, and an HRP-conjugated goat anti-rabbit antibody (1:5000 dilution; Promega, #W4011) was used as a secondary antibody.

Binding antibody multiplexed assay

Multiplex antibody binding assay was performed as previously described to measure the breadth of serum antibody binding (*68*) using a panel of HIV Env proteins including the following: 1086C. gp120 (*69*), MN. gp120 gDneg (clade B) (*9*), A244 gp120 gDneg (Clade AE) (*9*), A1.con.env03 gp140 (consensus clade A Env gp140 with deletions in the gp41 cleavage site and fusion domain) (*8*), and B.con.env03 gp140 (consensus clade B Env gp140) (*9*). The plates were read on Bio-Plex 200 System (Bio-Rad Laboratories Inc.), and the results were expressed as median fluorescence intensity (MFI).

Infected cell antibody binding assay

Indirect surface staining was used to measure the ability of rabbit serum antibodies to bind HIV-1 Env expressed on the surface of infected cells. Binding was assessed by a previously described indirect surface staining approach (*34*) using CEM.NKR$_{CCR5}$ cells [National Institutes of Health (NIH) AIDS Reagent Program from A. Trkola (*70*)] infected with the CH505T/F infectious molecular clone virus or mock infected cells. The cells were then incubated with a 1:100 dilution of serum samples for 2 hours at 37°C and then stained with LIVE/DEAD Aqua Dead Cell Stain (Thermo Fisher Scientific, #L34966), followed by permeabilization with Cytofix/Cytoperm solution (BD Biosciences, #554714) before staining with RD1-conjugated anti-p24 MAb KC57 (Beckman Coulter Inc., #6604667) and fluorescein isothiocyanate (FITC)–conjugated anti-rabbit IgG (H+L) (Southern Biotech, #4041-02). The result was read by flow cytometry; cells positive for serum antibody binding were defined as $p24^+$ $FITC^+$ and viable. Final results were reported as the change in FITC MFI or frequency of positive cells for postvaccination samples compared to the prevaccination sample after subtraction of the corresponding data from cells stained with secondary antibody alone and staining of mock-infected cells.

TZM-bl cell neutralization assay

Neutralizing antibody titers in rabbits were measured with the previously described standardized TZM-bl cell assay (*71*). Briefly, serially threefold diluted rabbit plasma samples from 1:20 to 1:43740 were incubated with HIV pseudovirus of interest, and then, a 1- to 1.5-hour incubation at 37°C and 5% CO_2 was given to allow neutralization to occur. *O*-(diethylaminoethyl)–dextran (10 μg/ml; Sigma-Aldrich, #D9885) and 1×10^5 TZM-bl cells (NIH AIDS Reagent Program, #8129) were added to each well. After 48 hours of incubation at 37°C and 5% CO_2, 150 μl of medium was removed from each well, followed by adding 100 μl of Bright-Glo luciferase substrate (Promega, #E264CX) to each well. A total of 150 μl of the mixture was transferred to Corning 96-well flat-bottom black plates (VWR, #29444-018). The intensity of luminescence was measured on Victor X3 Multilabel Plate Reader (PerkinElmer).

Antibody-dependent cellular phagocytosis

ADCP assay was performed as previously described (*41*, *42*) using HIV Env antigens (HIV CH505T/F gp120 and HIV 1086.C K160N gp120) covalently bound to NeutrAvidin-labeled fluorescent microspheres (Invitrogen, #F8776). Briefly, plasma was diluted to 1:50 dilution when incubated with antigen-coupled beads and human-derived monocyte cell line, THP-1 cells (American Type Culture Collection, TIB-201) under 1200*g* centrifugation for 1 hour at 4°C, followed by another hour of incubation at 37°C to allow phagocytosis to occur. THP-1 cells then were fixed with 2% paraformaldehyde (Sigma-Aldrich, #158127), and fluorescence of the cells was assessed using flow cytometry (BD, Fortessa). Phagocytosis scores were calculated by multiplying the MFI and frequency of bead-positive cells and dividing by the MFI and frequency of bead-positive cells in the no-antibody control (PBS). All plasma samples were tested in two independent assays, and the average phagocytosis scores from these two independent assays were reported.

ADCC against HIV Env-coated target cells

The ADCC-GranToxiLux assay was performed as previously described (*72*, *73*), using as target cells a clonal isolate of the CEM.NKR$_{CCR5}$ $CD4^+$ T cell line coated with CH505T/F gp120 Env protein (*74*). Human peripheral blood mononuclear cell (PBMC) effector cells were obtained from leukapheresis of an HIV-seronegative donor (*75*) and used at an effector cell–to–target cell ratio of 30:1. Serum samples were tested at fourfold serial dilutions starting at 1:100. Data were reported as the maximum proportion of cells positive for proteolytically active granzyme B (GzB) out of the total viable target cell population (maximum %GzB activity) after subtracting the background activity observed in wells containing effector and target cells in the absence of plasma. ADCC end point titers were determined by interpolating the last serum dilution above the previously established positive cutoff for this assay (8% GzB activity) and were reported as reciprocal dilution.

ADCC against HIV-infected target cells

ADCC activity directed against HIV-infected target cells was determined by the ADCC-luciferase assay as previously described (*34*, *76*). CEM.NKR$_{CCR5}$ target cells were infected with infectious molecular clone virus encoding *Renilla* luciferase (*77*) and expressing the HIV-1 CH505T/F Env (*74*). Target cells were incubated with human PBMC effector cells (*75*) that had been treated overnight with IL-15 (10 ng/ml; 30:1 effector cell–to–target cell ratio), and serial dilutions of serum in half-area opaque flat-bottom plates (Corning Life Sciences, #3697) in duplicate wells. Plates were incubated for 6 hours at 37°C and 5% CO_2. ADCC activity, reported as percent specific killing, was calculated from the change in relative light units (RLU; ViviRen luciferase assay; Promega, #E649A) resulting from the loss of intact target cells in wells containing effector cells, target cells, and serum samples compared to RLU in control wells containing target cells and effector cells alone according to the following formula: percent specific killing = [(number of RLU of target and effector well − number of RLU of test well)/number of RLU of target and effector well] × 100. ADCC end point titers were determined by interpolating the last serum dilution above the positive cutoff for this assay (15% specific killing) after subtracting the background activity observed for matched prevaccination samples and were reported as reciprocal dilution.

IgG Fc N-linked glycan analysis

We modified a previously reported protocol for the enrichment of gp120-specific IgG Fc region, (*14*). Briefly, CH505T/F gp120 (or 1086.C K160N gp120 for mouse sera) was first biotinylated using EZ-Link NHS-LC-LC-Biotin (Thermo Fisher Scientific, #21323) at

a 1:20 protein-to-biotin molar ratio. Biotinylated gp120 was incubated with streptavidin magnetic beads (NEB, #S1420S); then, unbound gp120 in the supernatant was removed by two washes of the magnetic beads with washing buffer (0.5 M NaCl, 20 mM tris-HCl, and 1 mM EDTA; pH 7.5). Schematic of this procedure is summarized in fig. S7. A total of 200 µl of serum sample was first incubated with 100 µl of antigen-free magnetic beads to pull down nonspecific binding serum glycoproteins. The precleaned serum was then incubated with 200 µl of the gp120-coupled beads at 4°C overnight to allow binding of gp120-specific antibodies. Rabbit IgG Fc region was released by incubating antibody-bound beads with IdeZ (NEB, #P0770S) at 37°C for an hour and 2 hours with FabULOUS enzyme (Genovis, #A0-PU1-020) for mouse IgG. Total serum IgG was purified with excessing amount of protein A on Protein A HP MultiTrap (Cytiva, #28903133). After digestion with IgG protease, the Fc region was separated from Fab with Protein A HP MultiTrap. The procedure of deglycosylation and glycan labeling was conducted following the manufacturer's instructions (Agilent Technologies Inc., #GX96-IQ). Buffer exchange to 20 mM Hepes was applied to remove tris-HCl in the IgG protease buffer. The labeled glycans were analyzed using the Gly-Q Glycan Analysis System GQ2100 (ProZyme now Agilent Technologies Inc.). To minimize human influence in the data processing, the relative abundance of each glycan species was automatically generated by the built-in software. The relative abundance of each glycan species was calculated by dividing the peak area of a given glycan with the area of the all peaks on the electropherogram summed up together: relative abundance = (peak area of a glycan/area summation of all peaks observed) × 100. For glycan species that were only absent in a subset of samples, their relative abundance was manually set to the detection cutoff of 0.05% peak area.

Statistical analysis

For the ELISA data, we ran a linear mixed effects model, with fixed effects for vaccine, booster period, baseline values (value at week 0, before vaccination) and time in weeks along with nested random effects for individual rabbit by booster period. Testing of the fixed effects was via analysis of variance (ANOVA). We performed the analysis in R using the lme4 and lmerTest packages. The binding antibody multiplexed assay (BAMA) data were presented with a box plot, where the boxes indicate the 25th to 75th percentiles with a middle bar presenting the group mean and error presenting the range (format is applied to other box plots throughout this paper). BAMA data were analyzed using generalized estimating equations (GEEs), testing for the interaction between vaccine and time while adjusting for antigen. We used bias-corrected SE estimators to account for the small sample size (*78*) and evaluated the resulting Wald test statistics. Multiple testing correction within the BAMA data was done via Bonferroni at 0.05. In addition, we used GEE for ADCP analyses, although, here, we tested for an interaction between vaccine and the antibody being measured (while normalized with time and baseline value at week 0). Again, the multiple testing of the vaccine across the three antibodies was done via Bonferroni. All the above data was $\log_{10}$-transformed before analysis. For other repeated measures analyses, we used a nonparametric repeated measures test as the data either had small sample sizes or were non-normal. Permutation tests were used when the resulting covariance matrix was singular. For all other single analyses, we used Wilcoxon rank sum test via the coin package in R to calculate the exact *P* values; multiple testing corrections for these single analyses were via Benjamini Hochberg false discovery rate (FDR; done within assay). Difference was considered statistically significant when unadjusted $P < 0.05$ and multiple testing–adjusted FDR $P < 0.1$. CIs for reported Spearman correlations were done using the rcompanion package.

SUPPLEMENTARY MATERIALS

Supplementary material for this article is available at https://science.org/doi/10.1126/sciadv.abq0273

View/request a protocol for this paper from *Bio-protocol*.

REFERENCES AND NOTES

1. L. Corey, P. B. Gilbert, G. D. Tomaras, B. F. Haynes, G. Pantaleo, A. S. Fauci, Immune correlates of vaccine protection against HIV-1 acquisition. *Sci. Transl. Med.* **7**, 310rv7 (2015).
2. D. J. DiLillo, G. S. Tan, P. Palese, J. V. Ravetch, Broadly neutralizing hemagglutinin stalk-specific antibodies require FcγR interactions for protection against influenza virus in vivo. *Nat. Med.* **20**, 143–151 (2014).
3. S. Kohl, L. S. Loo, Protection of neonatal mice against herpes simplex virus infection: Probable in vivo antibody-dependent cellular cytotoxicity. *J. Immunol.* **129**, 370–376 (1982).
4. K. L. Warfield, D. L. Swenson, G. G. Olinger, W. V. Kalina, M. J. Aman, S. Bavari, Ebola virus-like particle-based vaccine protects nonhuman primates against lethal Ebola virus challenge. *J Infect. Dis.* **196** Suppl 2, S430–S437 (2007).
5. J. A. Jenks, C. S. Nelson, H. K. Roark, M. L. Goodwin, R. F. Pass, D. I. Bernstein, E. B. Walter, K. M. Edwards, D. Wang, T. M. Fu, Z. An, C. Chan, S. R. Permar, Antibody binding to native cytomegalovirus glycoprotein B predicts efficacy of the gB/MF59 vaccine in humans. *Sci. Transl. Med.* **12**, eabb3611 (2020).
6. C. S. Nelson, T. Huffman, J. A. Jenks, E. Cisneros de la Rosa, G. Xie, N. Vandergrift, R. F. Pass, J. Pollara, S. R. Permar, HCMV glycoprotein B subunit vaccine efficacy mediated by nonneutralizing antibody effector functions. *Proc. Natl. Acad. Sci. U.S.A.* **115**, 6267–6272 (2018).
7. D. R. Burton, L. Hangartner, Broadly neutralizing antibodies to HIV and their role in vaccine design. *Annu. Rev. Immunol.* **34**, 635–659 (2016).
8. B. F. Haynes, P. B. Gilbert, M. J. McElrath, S. Zolla-Pazner, G. D. Tomaras, S. M. Alam, D. T. Evans, D. C. Montefiori, C. Karnasuta, R. Sutthent, H. X. Liao, A. L. DeVico, G. K. Lewis, C. Williams, A. Pinter, Y. Fong, H. Janes, A. DeCamp, Y. Huang, M. Rao, E. Billings, N. Karasavvas, M. L. Robb, V. Ngauy, M. S. de Souza, R. Paris, G. Ferrari, R. T. Bailer, K. A. Soderberg, C. Andrews, P. W. Berman, N. Frahm, S. C. De Rosa, M. D. Alpert, N. L. Yates, X. Shen, R. A. Koup, P. Pitisuttithum, J. Kaewkungwal, S. Nitayaphan, S. Rerks-Ngarm, N. L. Michael, J. H. Kim, Immune-correlates analysis of an HIV-1 vaccine efficacy trial. *N. Engl. J. Med.* **366**, 1275–1286 (2012).
9. S. Rerks-Ngarm, P. Pitisuttithum, S. Nitayaphan, J. Kaewkungwal, J. Chiu, R. Paris, N. Premsri, C. Namwat, M. de Souza, E. Adams, M. Benenson, S. Gurunathan, J. Tartaglia, J. G. McNeil, D. P. Francis, D. Stablein, D. L. Birx, S. Chunsuttiwat, C. Khamboonruang, P. Thongcharoen, M. L. Robb, N. L. Michael, P. Kunasol, J. H. Kim; MOPH-TAVEG Investigators, Vaccination with ALVAC and AIDSVAX to prevent HIV-1 infection in Thailand. *N. Engl. J. Med.* **361**, 2209–2220 (2009).
10. G. E. Gray, L. G. Bekker, F. Laher, M. Malahleha, M. Allen, Z. Moodie, N. Grunenberg, Y. Huang, D. Grove, B. Prigmore, J. J. Kee, D. Benkeser, J. Hural, C. Innes, E. Lazarus, G. Meintjes, N. Naicker, D. Kalonji, M. Nchabeleng, M. Sebe, N. Singh, P. Kotze, S. Kassim, T. Dubula, V. Naicker, W. Brumskine, C. N. Ncayiya, A. M. Ward, N. Garrett, G. Kistnasami, Z. Gaffoor, P. Selepe, P. B. Makhoba, M. P. Mathebula, P. Mda, T. Adonis, K. S. Mapetla, B. Modibedi, T. Philip, G. Kobane, C. Bentley, S. Ramirez, S. Takuva, M. Jones, M. Sikhosana, M. Atujuna, M. Andrasik, N. S. Hejazi, A. Puren, L. Wiesner, S. Phogat, C. D. Granados, M. Koutsoukos, O. Van Der Meeren, S. W. Barnett, N. Kanesa-Thasan, J. G. Kublin, M. J. McElrath, P. B. Gilbert, H. Janes, L. Corey; HVTN 702 Study Team, Vaccine efficacy of ALVAC-HIV and bivalent subtype C gp120-MF59 in adults. *N. Engl. J. Med.* **384**, 1089–1100 (2021).
11. M. E. Ackerman, M. Crispin, X. Yu, K. Baruah, A. W. Boesch, D. J. Harvey, A. S. Dugast, E. L. Heizen, A. Ercan, I. Choi, H. Streeck, P. A. Nigrovic, C. Bailey-Kellogg, C. Scanlan, G. Alter, Natural variation in Fc glycosylation of HIV-specific antibodies impacts antiviral activity. *J. Clin. Invest.* **123**, 2183–2192 (2013).
12. M. E. Ackerman, A.-S. Dugast, E. G. McAndrew, S. Tsoukas, A. F. Licht, D. J. Irvine, G. Alter, Enhanced phagocytic activity of HIV-specific antibodies correlates with natural production of immunoglobulins with skewed affinity for FcγR2a and FcγR2b. *J. Virol.* **87**, 5468–5476 (2013).
13. M. F. Jennewein, G. Alter, The immunoregulatory roles of antibody glycosylation. *Trends Immunol.* **38**, 358–372 (2017).

14. G. Lofano, M. J. Gorman, A. S. Yousif, W. H. Yu, J. M. Fox, A. S. Dugast, M. E. Ackerman, T. J. Suscovich, J. Weiner, D. Barouch, H. Streeck, S. Little, D. Smith, D. Richman, D. Lauffenburger, B. D. Walker, M. S. Diamond, G. Alter, Antigen-specific antibody Fc glycosylation enhances humoral immunity via the recruitment of complement. *Sci. Immunol.* **3**, eaat7796 (2018).
15. T. T. Wang, J. V. Ravetch, Functional diversification of IgGs through Fc glycosylation. *J. Clin. Investig.* **129**, 3492–3498 (2019).
16. Y. C. Bartsch, S. Eschweiler, A. Leliavski, H. B. Lunding, S. Wagt, J. Petry, G.-M. Lilienthal, J. Rahmöller, N. de Haan, A. Hölscher, IgG Fc sialylation is regulated during the germinal center reaction following immunization with different adjuvants. *J. Allergy Clin. Immunol.* **146**, 652–666. e11 (2020).
17. C. N. Fries, E. J. Curvino, J.-L. Chen, S. R. Permar, G. G. Fouda, J. H. Collier, Advances in nanomaterial vaccine strategies to address infectious diseases impacting global health. *Nat. Nanotechnol.* **16**, 1–14 (2021).
18. P. Martinez-Murillo, K. Tran, J. Guenaga, G. Lindgren, M. Adori, Y. Feng, G. E. Phad, N. Vazquez Bernat, S. Bale, J. Ingale, V. Dubrovskaya, S. O'Dell, L. Pramanik, M. Spangberg, M. Corcoran, K. Lore, J. R. Mascola, R. T. Wyatt, G. B. Karlsson Hedestam, Particulate array of well-ordered HIV clade C Env trimers elicits neutralizing antibodies that display a unique V2 cap approach. *Immunity* **46**, 804–817.e7 (2017).
19. K. Sliepen, G. Ozorowski, J. A. Burger, T. van Montfort, M. Stunnenberg, C. LaBranche, D. C. Montefiori, J. P. Moore, A. B. Ward, R. W. Sanders, Presenting native-like HIV-1 envelope trimers on ferritin nanoparticles improves their immunogenicity. *Retrovirology* **12**, 82 (2015).
20. K. O. Saunders, K. Wiehe, M. Tian, P. Acharya, T. Bradley, S. M. Alam, E. P. Go, R. Scearce, L. Sutherland, R. Henderson, A. L. Hsu, M. J. Borgnia, H. Chen, X. Lu, N. R. Wu, B. Watts, C. Jiang, D. Easterhoff, H. L. Cheng, K. McGovern, P. Waddicor, A. Chapdelaine-Williams, A. Eaton, J. Zhang, W. Rountree, L. Verkoczy, M. Tomai, M. G. Lewis, H. R. Desaire, R. J. Edwards, D. W. Cain, M. Bonsignori, D. Montefiori, F. W. Alt, B. F. Haynes, Targeted selection of HIV-specific antibody mutations by engineering B cell maturation. *Science* **366**, eaay7199 (2019).
21. J. Chen, R. R. Pompano, F. W. Santiago, L. Maillat, R. Sciammas, T. Sun, H. Han, D. J. Topham, A. S. Chong, J. H. Collier, The use of self-adjuvanting nanofiber vaccines to elicit high-affinity B cell responses to peptide antigens without inflammation. *Biomaterials* **34**, 8776–8785 (2013).
22. C. Mora-Solano, Y. Wen, H. Han, J. Chen, A. S. Chong, M. L. Miller, R. R. Pompano, J. H. Collier, Active immunotherapy for TNF-mediated inflammation using self-assembled peptide nanofibers. *Biomaterials* **149**, 1–11 (2017).
23. J. S. Rudra, T. Sun, K. C. Bird, M. D. Daniels, J. Z. Gasiorowski, A. S. Chong, J. H. Collier, Modulating adaptive immune responses to peptide self-assemblies. *ACS Nano* **6**, 1557–1564 (2012).
24. L. S. Shores, S. H. Kelly, K. M. Hainline, J. Suwanpradid, A. S. MacLeod, J. H. Collier, Multifactorial design of a supramolecular peptide anti-IL-17 vaccine toward the treatment of psoriasis. *Front. Immunol.* **11**, 1855 (2020).
25. Y. Si, Y. Wen, S. H. Kelly, A. S. Chong, J. H. Collier, Intranasal delivery of adjuvant-free peptide nanofibers elicits resident $CD8^+$ T cell responses. *J. Control. Release* **282**, 120–130 (2018).
26. G. A. Hudalla, J. A. Modica, Y. F. Tian, J. S. Rudra, A. S. Chong, T. Sun, M. Mrksich, J. H. Collier, A self-adjuvanting supramolecular vaccine carrying a folded protein antigen. *Adv. Healthc. Mater.* **2**, 1114–1119 (2013).
27. J. S. Rudra, Y. F. Tian, J. P. Jung, J. H. Collier, A self-assembling peptide acting as an immune adjuvant. *Proc. Natl. Acad. Sci.* **107**, 622–627 (2010).
28. G. A. Hudalla, T. Sun, J. Z. Gasiorowski, H. Han, Y. F. Tian, A. S. Chong, J. H. Collier, Gradated assembly of multiple proteins into supramolecular nanomaterials. *Nat. Mater.* **13**, 829–836 (2014).
29. R. R. Pompano, J. Chen, E. A. Verbus, H. Han, A. Fridman, T. McNeely, J. H. Collier, A. S. Chong, Titrating T-cell epitopes within self-assembled vaccines optimizes CD4+ helper T cell and antibody outputs. *Adv. Healthc. Mater.* **3**, 1898–1908 (2014).
30. T. Tokatlian, B. J. Read, C. A. Jones, D. W. Kulp, S. Menis, J. Y. H. Chang, J. M. Steichen, S. Kumari, J. D. Allen, E. L. Dane, A. Liguori, M. Sangesland, D. Lingwood, M. Crispin, W. R. Schief, D. J. Irvine, Innate immune recognition of glycans targets HIV nanoparticle immunogens to germinal centers. *Science* **363**, 649–654 (2019).
31. N. R. Bennett, D. B. Zwick, A. H. Courtney, L. L. Kiessling, Multivalent antigens for promoting B and T cell activation. *ACS Chem. Biol.* **10**, 1817–1824 (2015).
32. Y. Kato, R. K. Abbott, B. L. Freeman, S. Haupt, B. Groschel, M. Silva, S. Menis, D. J. Irvine, W. R. Schief, S. Crotty, Multifaceted effects of antigen valency on b cell response composition and differentiation in vivo. *Immunity* **53**, 548–563.e8 (2020).
33. C. N. Fries, J. L. Chen, M. L. Dennis, N. L. Votaw, J. Eudailey, B. E. Watts, K. M. Hainline, D. W. Cain, R. Barfield, C. Chan, M. A. Moody, B. F. Haynes, K. O. Saunders, S. R. Permar, G. G. Fouda, J. H. Collier, HIV envelope antigen valency on peptide nanofibers modulates antibody magnitude and binding breadth. *Sci. Rep.* **11**, 14494 (2021).
34. J. Pollara, D. I. Jones, T. Huffman, R. W. Edwards, M. Dennis, S. H. Li, S. Jha, D. Goodman, A. Kumar, C. C. LaBranche, D. C. Montefiori, G. G. Fouda, T. J. Hope, G. D. Tomaras, H. F. Staats, G. Ferrari, S. R. Permar, Bridging vaccine-induced HIV-1 neutralizing and effector antibody responses in rabbit and rhesus macaque animal models. *J. Virol.* **93**, e02119-e02118 (2019).
35. K. M. Hainline, L. S. Shores, N. L. Votaw, Z. J. Bernstein, S. H. Kelly, C. N. Fries, M. S. Madhira, C. A. Gilroy, A. Chilkoti, J. H. Collier, Modular complement assemblies for mitigating inflammatory conditions. *Proc. Natl. Acad. Sci. U.S.A.* **118**, e2018627118 (2021).
36. C. S. Theile, M. D. Witte, A. E. Blom, L. Kundrat, H. L. Ploegh, C. P. Guimaraes, Site-specific N-terminal labeling of proteins using sortase-mediated reactions. *Nat. Protoc.* **8**, 1800–1807 (2013).
37. S. P. Kasturi, M. A. U. Rasheed, C. Havenar-Daughton, M. Pham, T. Legere, Z. J. Sher, Y. Kovalenkov, S. Gumber, J. Y. Huang, R. Gottardo, W. Fulp, A. Sato, S. Sawant, S. Stanfield-Oakley, N. Yates, C. LaBranche, S. M. Alam, G. Tomaras, G. Ferrari, D. Montefiori, J. Wrammert, F. Villinger, M. Tomai, J. Vasilakos, C. B. Fox, S. G. Reed, B. F. Haynes, S. Crotty, R. Ahmed, B. Pulendran, 3M-052, a synthetic TLR-7/8 agonist, induces durable HIV-1 envelope-specific plasma cells and humoral immunity in nonhuman primates. *Sci. Immunol.* **5**, eabb1025 (2020).
38. M. Silva, Y. Kato, M. B. Melo, I. Phung, B. L. Freeman, Z. Li, K. Roh, J. W. Van Wijnbergen, H. Watkins, C. A. Enemuo, B. L. Hartwell, J. Y. H. Chang, S. Xiao, K. A. Rodrigues, K. M. Cirelli, N. Li, S. Haupt, A. Aung, B. Cossette, W. Abraham, S. Kataria, R. Bastidas, J. Bhiman, C. Linde, N. I. Bloom, B. Groschel, E. Georgeson, N. Phelps, A. Thomas, J. Bals, D. G. Carnathan, D. Lingwood, D. R. Burton, G. Alter, T. P. Padera, A. M. Belcher, W. R. Schief, G. Silvestri, R. M. Ruprecht, S. Crotty, D. J. Irvine, A particulate saponin/TLR agonist vaccine adjuvant alters lymph flow and modulates adaptive immunity. *Sci. Immunol.* **6**, eabf1152 (2021).
39. M. A. Moody, S. Santra, N. A. Vandergrift, L. L. Sutherland, T. C. Gurley, M. S. Drinker, A. A. Allen, S. M. Xia, R. R. Meyerhoff, R. Parks, K. E. Lloyd, D. Easterhoff, S. M. Alam, H. X. Liao, B. M. Ward, G. Ferrari, D. C. Montefiori, G. D. Tomaras, R. A. Seder, N. L. Letvin, B. F. Haynes, Toll-like receptor 7/8 (TLR7/8) and TLR9 agonists cooperate to enhance HIV-1 envelope antibody responses in rhesus macaques. *J. Virol.* **88**, 3329–3339 (2014).
40. W. B. Williams, J. Zhang, C. Jiang, N. I. Nicely, D. Fera, K. Luo, M. A. Moody, H. X. Liao, S. M. Alam, T. B. Kepler, A. Ramesh, K. Wiehe, J. A. Holland, T. Bradley, N. Vandergrift, K. O. Saunders, R. Parks, A. Foulger, S. M. Xia, M. Bonsignori, D. C. Montefiori, M. Louder, A. Eaton, S. Santra, R. Scearce, L. Sutherland, A. Newman, H. Bouton-Verville, C. Bowman, H. Bomze, F. Gao, D. J. Marshall, J. F. Whitesides, X. Nie, G. Kelsoe, S. G. Reed, C. B. Fox, K. Clary, M. Koutsoukos, D. Franco, J. R. Mascola, S. C. Harrison, B. F. Haynes, L. Verkoczy, Initiation of HIV neutralizing B cell lineages with sequential envelope immunizations. *Nat. Commun.* **8**, 1732 (2017).
41. M. Z. Tay, P. Liu, L. D. Williams, M. D. McRaven, S. Sawant, T. C. Gurley, T. T. Xu, S. M. Dennison, H.-X. Liao, A.-L. Chenine, S. M. Alam, M. A. Moody, T. J. Hope, B. F. Haynes, G. D. Tomaras, Antibody-mediated internalization of infectious HIV-1 virions differs among antibody isotypes and subclasses. *PLOS Pathog.* **12**, e1005817 (2016).
42. M. E. Ackerman, B. Moldt, R. T. Wyatt, A.-S. Dugast, E. McAndrew, S. Tsoukas, S. Jost, C. T. Berger, G. Sciaranghella, Q. Liu, D. J. Irvine, D. R. Burton, G. Alter, A robust, high-throughput assay to determine the phagocytic activity of clinical antibody samples. *J. Immunol. Methods* **366**, 8–19 (2011).
43. K. O. Saunders, L. K. Verkoczy, C. Jiang, J. Zhang, R. Parks, H. Chen, M. Housman, H. Bouton-Verville, X. Shen, A. M. Trama, R. Scearce, L. Sutherland, S. Santra, A. Newman, A. Eaton, K. Xu, I. S. Georgiev, M. G. Joyce, G. D. Tomaras, M. Bonsignori, S. G. Reed, A. Salazar, J. R. Mascola, M. A. Moody, D. W. Cain, M. Centlivre, S. Zurawski, G. Zurawski, H. P. Erickson, P. D. Kwong, S. M. Alam, Y. Levy, D. C. Montefiori, B. F. Haynes, Vaccine induction of heterologous Tier 2 HIV-1 neutralizing antibodies in animal models. *Cell Rep.* **21**, 3681–3690 (2017).
44. A. W. Chung, G. Alter, Systems serology: Profiling vaccine induced humoral immunity against HIV. *Retrovirology* **14**, 57 (2017).
45. A. E. Mahan, J. Tedesco, K. Dionne, K. Baruah, H. D. Cheng, P. L. De Jager, D. H. Barouch, T. Suscovich, M. Ackerman, M. Crispin, G. Alter, A method for high-throughput, sensitive analysis of IgG Fc and Fab glycosylation by capillary electrophoresis. *J. Immunol. Methods* **417**, 34–44 (2015).
46. J. Weber, H. Peng, C. Rader, From rabbit antibody repertoires to rabbit monoclonal antibodies. *Exp. Mol. Med.* **49**, e305 (2017).
47. R. L. Shields, J. Lai, R. Keck, L. Y. O'Connell, K. Hong, Y. G. Meng, S. H. Weikert, L. G. Presta, Lack of fucose on human IgG1 N-linked oligosaccharide improves binding to human Fcgamma RIII and antibody-dependent cellular toxicity. *J. Biol. Chem.* **277**, 26733–26740 (2002).
48. T. Shinkawa, K. Nakamura, N. Yamane, E. Shoji-Hosaka, Y. Kanda, M. Sakurada, K. Uchida, H. Anazawa, M. Satoh, M. Yamasaki, N. Hanai, K. Shitara, The absence of fucose but not the presence of galactose or bisecting N-acetylglucosamine of human IgG1 complex-type oligosaccharides shows the critical role of enhancing antibody-dependent cellular cytotoxicity. *J. Biol. Chem.* **278**, 3466–3473 (2003).
49. T. T. Junttila, K. Parsons, C. Olsson, Y. Lu, Y. Xin, J. Theriault, L. Crocker, O. Pabonan, T. Baginski, G. Meng, K. Totpal, R. F. Kelley, M. X. Sliwkowski, Superior in vivo efficacy

of afucosylated trastuzumab in the treatment of HER2-amplified breast cancer. *Cancer Res.* **70**, 4481–4489 (2010).
50. E. Corrales-Aguilar, M. Trilling, H. Reinhard, E. Merce-Maldonado, M. Widera, H. Schaal, A. Zimmermann, O. Mandelboim, H. Hengel, A novel assay for detecting virus-specific antibodies triggering activation of Fcγ receptors. *J. Immunol. Methods* **387**, 21–35 (2013).
51. R. K. Abbott, S. Crotty, Factors in B cell competition and immunodominance. *Immunol. Rev.* **296**, 120–131 (2020).
52. M. F. Bachmann, G. T. Jennings, Vaccine delivery: A matter of size, geometry, kinetics and molecular patterns. *Nat. Rev. Immunol.* **10**, 787–796 (2010).
53. R. Veneziano, T. J. Moyer, M. B. Stone, E.-C. Wamhoff, B. J. Read, S. Mukherjee, T. R. Shepherd, J. Das, W. R. Schief, D. J. Irvine, M. Bathe, Role of nanoscale antigen organization on B-cell activation probed using DNA origami. *Nat. Nanotechnol.* **15**, 716–723 (2020).
54. T. W. Baba, V. Liska, R. Hofmann-Lehmann, J. Vlasak, W. Xu, S. Ayehunie, L. A. Cavacini, M. R. Posner, H. Katinger, G. Stiegler, B. J. Bernacky, T. A. Rizvi, R. Schmidt, L. R. Hill, M. E. Keeling, Y. Lu, J. E. Wright, T. C. Chou, R. M. Ruprecht, Human neutralizing monoclonal antibodies of the IgG1 subtype protect against mucosal simian-human immunodeficiency virus infection. *Nat. Med.* **6**, 200–206 (2000).
55. A. J. Hessell, E. G. Rakasz, D. M. Tehrani, M. Huber, K. L. Weisgrau, G. Landucci, D. N. Forthal, W. C. Koff, P. Poignard, D. I. Watkins, D. R. Burton, Broadly neutralizing monoclonal antibodies 2F5 and 4E10 directed against the human immunodeficiency virus type 1 gp41 membrane-proximal external region protect against mucosal challenge by simian-human immunodeficiency virus SHIVBa-L. *J. Virol.* **84**, 1302–1313 (2010).
56. P. W. Parren, P. A. Marx, A. J. Hessell, A. Luckay, J. Harouse, C. Cheng-Mayer, J. P. Moore, D. R. Burton, Antibody protects macaques against vaginal challenge with a pathogenic R5 simian/human immunodeficiency virus at serum levels giving complete neutralization in vitro. *J. Virol.* **75**, 8340–8347 (2001).
57. J. R. Mascola, G. Stiegler, T. C. VanCott, H. Katinger, C. B. Carpenter, C. E. Hanson, H. Beary, D. Hayes, S. S. Frankel, D. L. Birx, M. G. Lewis, Protection of macaques against vaginal transmission of a pathogenic HIV-1/SIV chimeric virus by passive infusion of neutralizing antibodies. *Nat. Med.* **6**, 207–210 (2000).
58. A. J. Hessell, P. Poignard, M. Hunter, L. Hangartner, D. M. Tehrani, W. K. Bleeker, P. W. H. I. Parren, P. A. Marx, D. R. Burton, Effective, low-titer antibody protection against low-dose repeated mucosal SHIV challenge in macaques. *Nat. Med.* **15**, 951–954 (2009).
59. L. Corey, P. B. Gilbert, M. Juraska, D. C. Montefiori, L. Morris, S. T. Karuna, S. Edupuganti, N. M. Mgodi, A. C. deCamp, E. Rudnicki, Y. Huang, P. Gonzales, R. Cabello, C. Orrell, J. R. Lama, F. Laher, E. M. Lazarus, J. Sanchez, I. Frank, J. Hinojosa, M. E. Sobieszczyk, K. E. Marshall, P. G. Mukwekwerere, J. Makhema, L. R. Baden, J. I. Mullins, C. Williamson, J. Hural, M. J. McElrath, C. Bentley, S. Takuva, M. M. G. Lorenzo, D. N. Burns, N. Espy, A. K. Randhawa, N. Kochar, E. Piwowar-Manning, D. J. Donnell, N. Sista, P. Andrew, J. G. Kublin, G. Gray, J. E. Ledgerwood, J. R. Mascola, M. S. Cohen; for the HVTN 704/HPTN 085 and HVTN 703/HPTN 081 Study Teams, Two randomized trials of neutralizing antibodies to prevent HIV-1 acquisition. *N. Engl. J. Med.* **384**, 1003–1014 (2021).
60. D. C. Montefiori, C. Karnasuta, Y. Huang, H. Ahmed, P. Gilbert, M. S. de Souza, R. McLinden, S. Tovanabutra, A. Laurence-Chenine, E. Sanders-Buell, M. A. Moody, M. Bonsignori, C. Ochsenbauer, J. Kappes, H. Tang, K. Greene, H. Gao, C. C. LaBranche, C. Andrews, V. R. Polonis, S. Rerks-Ngarm, P. Pitisuttithum, S. Nitayaphan, J. Kaewkungwal, S. G. Self, P. W. Berman, D. Francis, F. Sinangil, C. Lee, J. Tartaglia, M. L. Robb, B. F. Haynes, N. L. Michael, J. H. Kim, Magnitude and breadth of the neutralizing antibody response in the RV144 and Vax003 HIV-1 vaccine efficacy trials. *J. Infect. Dis.* **206**, 431–441 (2012).
61. T. Li, D. J. DiLillo, S. Bournazos, J. P. Giddens, J. V. Ravetch, L.-X. Wang, Modulating IgG effector function by Fc glycan engineering. *Proc. Natl. Acad. Sci. U.S.A.* **114**, 3485–3490 (2017).
62. N. A. Pereira, K. F. Chan, P. C. Lin, Z. Song, The "less-is-more" in therapeutic antibodies: Afucosylated anti-cancer antibodies with enhanced antibody-dependent cellular cytotoxicity. *MAbs* **10**, 693–711 (2018).
63. M. D. Larsen, E. L. de Graaf, M. E. Sonneveld, H. R. Plomp, J. Nouta, W. Hoepel, H. J. Chen, F. Linty, R. Visser, M. Brinkhaus, T. Šuštić, S. W. de Taeye, A. E. H. Bentlage, S. Toivonen, C. A. M. Koeleman, S. Sainio, N. A. Kootstra, P. J. M. Brouwer, C. E. Geyer, N. I. L. Derksen, G. Wolbink, M. de Winther, R. W. Sanders, M. J. van Gils, S. de Bruin, A. P. J. Vlaar; Amsterdam UMC COVID-19; Biobank Study Group, T. Rispens, J. den Dunnen, H. L. Zaaijer, M. Wuhrer, C. E. van der Schoot, G. Vidarsson, Afucosylated IgG characterizes enveloped viral responses and correlates with COVID-19 severity. *Science* **371**, (2021).
64. S. Chakraborty, J. Gonzalez, K. Edwards, V. Mallajosyula, A. S. Buzzanco, R. Sherwood, C. Buffone, N. Kathale, S. Providenza, M. M. Xie, J. R. Andrews, C. A. Blish, U. Singh, H. Dugan, P. C. Wilson, T. D. Pham, S. D. Boyd, K. C. Nadeau, B. A. Pinsky, S. Zhang, M. J. Memoli, J. K. Taubenberger, T. Morales, J. M. Schapiro, G. S. Tan, P. Jagannathan, T. T. Wang, Proinflammatory IgG Fc structures in patients with severe COVID-19. *Nat. Immunol.* **22**, 67–73 (2021).
65. W. Hoepel, H. J. Chen, C. E. Geyer, S. Allahverdiyeva, X. D. Manz, S. W. de Taeye, J. Aman, L. Mes, M. Steenhuis, G. R. Griffith, P. I. Bonta, P. J. M. Brouwer, T. G. Caniels, K. van der Straten, K. Golebski, R. E. Jonkers, M. D. Larsen, F. Linty, J. Nouta, C. van Roomen, F. van Baarle, C. M. van Drunen, G. Wolbink, A. P. J. Vlaar, G. J. de Bree, R. W. Sanders, L. Willemsen, A. E. Neele, D. van de Beek, T. Rispens, M. Wuhrer, H. J. Bogaard, M. J. van Gils, G. Vidarsson, M. de Winther, J. den Dunnen, High titers and low fucosylation of early human anti-SARS-CoV-2 IgG promote inflammation by alveolar macrophages. *Sci. Transl. Med.* **13**, eabf8654 (2021).
66. T. T. Wang, J. Sewatanon, M. J. Memoli, J. Wrammert, S. Bournazos, S. K. Bhaumik, B. A. Pinsky, K. Chokephaibulkit, N. Onlamoon, K. Pattanapanyasat, J. K. Taubenberger, R. Ahmed, J. V. Ravetch, IgG antibodies to dengue enhanced for FcγRIIIA binding determine disease severity. *Science* **355**, 395–398 (2017).
67. S. Bournazos, H. T. M. Vo, V. Duong, H. Auerswald, S. Ly, A. Sakuntabhai, P. Dussart, T. Cantaert, J. V. Ravetch, Antibody fucosylation predicts disease severity in secondary dengue infection. *Science* **372**, 1102–1105 (2021).
68. G. G. Fouda, C. K. Cunningham, E. J. McFarland, W. Borkowsky, P. Muresan, J. Pollara, L. Y. Song, B. E. Liebl, K. Whitaker, X. Shen, N. A. Vandergrift, R. G. Overman, N. L. Yates, M. A. Moody, C. Fry, J. H. Kim, N. L. Michael, M. Robb, P. Pitisuttithum, J. Kaewkungwal, S. Nitayaphan, S. Rerks-Ngarm, H. X. Liao, B. F. Haynes, D. C. Montefiori, G. Ferrari, G. D. Tomaras, S. R. Permar, Infant HIV type 1 gp120 vaccination elicits robust and durable anti-V1V2 immunoglobulin G responses and only rare envelope-specific immunoglobulin A responses. *J. Infect. Dis.* **211**, 508–517 (2015).
69. E. P. Go, H. X. Liao, S. M. Alam, D. Hua, B. F. Haynes, H. Desaire, Characterization of host-cell line specific glycosylation profiles of early transmitted/founder HIV-1 gp120 envelope proteins. *J. Proteome Res.* **12**, 1223–1234 (2013).
70. A. Trkola, J. Matthews, C. Gordon, T. Ketas, J. P. Moore, A cell line-based neutralization assay for primary human immunodeficiency virus type 1 isolates that use either the CCR5 or the CXCR4 coreceptor. *J. Virol.* **73**, 8966–8974 (1999).
71. M. Sarzotti-Kelsoe, R. T. Bailer, E. Turk, C. L. Lin, M. Bilska, K. M. Greene, H. Gao, C. A. Todd, D. A. Ozaki, M. S. Seaman, J. R. Mascola, D. C. Montefiori, Optimization and validation of the TZM-bl assay for standardized assessments of neutralizing antibodies against HIV-1. *J. Immunol. Methods* **409**, 131–146 (2014).
72. J. Pollara, L. Hart, F. Brewer, J. Pickeral, B. Z. Packard, J. A. Hoxie, A. Komoriya, C. Ochsenbauer, J. C. Kappes, M. Roederer, Y. Huang, K. J. Weinhold, G. D. Tomaras, B. F. Haynes, D. C. Montefiori, G. Ferrari, High-throughput quantitative analysis of HIV-1 and SIV-specific ADCC-mediating antibody responses. *Cytometry A* **79**, 603–612 (2011).
73. J. Pollara, C. Orlandi, C. Beck, R. W. Edwards, Y. Hu, S. Liu, S. Wang, R. A. Koup, T. N. Denny, S. Lu, G. D. Tomaras, A. DeVico, G. K. Lewis, G. Ferrari, Application of area scaling analysis to identify natural killer cell and monocyte involvement in the GranToxiLux antibody dependent cell-mediated cytotoxicity assay. *Cytometry A* **93**, 436–447 (2018).
74. H.-X. Liao, R. Lynch, T. Zhou, F. Gao, S. M. Alam, S. D. Boyd, A. Z. Fire, K. M. Roskin, C. A. Schramm, Z. Zhang, J. Zhu, L. Shapiro, N. C. S. Program, J. C. Mullikin, S. Gnanakaran, P. Hraber, K. Wiehe, G. Kelsoe, G. Yang, S.-M. Xia, D. C. Montefiori, R. Parks, K. E. Lloyd, R. M. Scearce, K. A. Soderberg, M. Cohen, G. Kamanga, M. K. Louder, L. M. Tran, Y. Chen, F. Cai, S. Chen, S. Moquin, X. Du, M. G. Joyce, S. Srivatsan, B. Zhang, A. Zheng, G. M. Shaw, B. H. Hahn, T. B. Kepler, B. T. Korber, P. D. Kwong, J. R. Mascola, B. F. Haynes, Co-evolution of a broadly neutralizing HIV-1 antibody and founder virus. *Nature* **496**, 469–476 (2013).
75. A. Garcia, S. Keinonen, A. M. Sanchez, G. Ferrari, T. N. Denny, M. A. Moody, Leukopak PBMC sample processing for preparing quality control material to support proficiency testing programs. *J. Immunol. Methods* **409**, 99–106 (2014).
76. L. Fisher, M. Zinter, S. Stanfield-Oakley, L. N. Carpp, R. W. Edwards, T. Denny, Z. Moodie, F. Laher, L. G. Bekker, M. J. McElrath, P. B. Gilbert, L. Corey, G. Tomaras, J. Pollara, G. Ferrari, Vaccine-induced antibodies mediate higher antibody-dependent cellular cytotoxicity after interleukin-15 pretreatment of natural killer effector cells. *Front. Immunol.* **10**, 2741 (2019).
77. T. G. Edmonds, H. Ding, X. Yuan, Q. Wei, K. S. Smith, J. A. Conway, L. Wieczorek, B. Brown, V. Polonis, J. T. West, D. C. Montefiori, J. C. Kappes, C. Ochsenbauer, Replication competent molecular clones of HIV-1 expressing Renilla luciferase facilitate the analysis of antibody inhibition in PBMC. *Virology* **408**, 1–13 (2010).
78. M. Wang, L. Kong, Z. Li, L. Zhang, Covariance estimators for generalized estimating equations (GEE) in longitudinal analysis with small samples. *Stat. Med.* **35**, 1706–1721 (2016).

Acknowledgments: We thank H. Hengel at University of Freiburg (Freiburg im Breisgau, Germany) for providing BW cell lines as a gift, and we would like to acknowledge Duke Biostatistics, Epidemiology and Research Design (BERD) Methods Core for performing statistical analyses and the Duke Human Vaccine Institute Biomolecular Interaction Analysis (BIA) Core Facility for performing SPR. **Funding:** This work was supported by Duke University MedX (to G.G.F. and J.H.C.), NIH grant 5R01AI145016-02 (to G.G.F. and J.H.C.), Duke University Center for AIDS Research (NIH-funded program) grant 5P30 AI064518 (to G.G.F. and J.H.C.), NIH training grant T32GM008555 (to C.N.F.), NSF Graduate Research Fellowship DGE-1644868 (to C.N.F.), and Duke University Interdisciplinary Research and Training Program in AIDS fellowship 5T32AI007392-31 (to S.J.B.). **Author contributions:** Conceptualization: J.-L.C.,

C.N.F., S.R.P., J.H.C., and G.G.F. Methodology: J.-L.C., C.N.F., S.H.L., and J.P. Investigation: J.L.-C., S.J.B., N.S.R., E.F.R., Y.W., R.J., B.W., and J.E. Resources: M.A.M., K.O.S., J.P., J.H.C., and G.G.F. Visualization: J.-L.C. and R.B. Formal analysis: R.B. and C.C. Supervision: C.C., S.R.P., J.H.C., and G.G.F. Funding acquisition: J.H.C. and G.G.F. Writing (original draft): J.-L.C. Writing (review and editing): J.-L.C., C.N.F., S.J.B., S.H.L., R.J., B.W., R.B., J.P., S.R.P., J.H.C., and G.G.F. **Competing interests:** S.R.P., J.H.C., K.O.S., C.N.F., and G.G.F. are inventors on a patent application related to this work filed by Duke University (no. US 20220040290A1, filed on 24 September 2019 and published on 10 February 2022). S.R.P. serves as a consultant for CMV vaccine programs at Merck, Pfizer, Moderna, Dynavax, and Hoopika and leads sponsored research programs with Merck and Moderna. The authors declare no other competing interests. **Data and materials availability:** All data needed to evaluate the conclusions in this paper are present in the paper and/or the Supplementary Materials. All data are available for download at https://zenodo.org/record/6672678 and https://github.com/rbarfield/gp120_rabbit.

Submitted 19 March 2022
Accepted 4 August 2022
Published 23 September 2022
10.1126/sciadv.abq0273